



HAL
open science

Nitric Oxide Remodels the Photosynthetic Apparatus upon S-Starvation in *Chlamydomonas reinhardtii*

Marcello de Mia, Stéphane Lemaire, Yves Choquet, Francis-André Wollman

► **To cite this version:**

Marcello de Mia, Stéphane Lemaire, Yves Choquet, Francis-André Wollman. Nitric Oxide Remodels the Photosynthetic Apparatus upon S-Starvation in *Chlamydomonas reinhardtii*. *Plant Physiology*, 2019, 179 (2), pp.718-731. 10.1104/pp.18.01164 . hal-02323489

HAL Id: hal-02323489

<https://hal.science/hal-02323489v1>

Submitted on 17 Nov 2020

HAL is a multi-disciplinary open access archive for the deposit and dissemination of scientific research documents, whether they are published or not. The documents may come from teaching and research institutions in France or abroad, or from public or private research centers.

L'archive ouverte pluridisciplinaire **HAL**, est destinée au dépôt et à la diffusion de documents scientifiques de niveau recherche, publiés ou non, émanant des établissements d'enseignement et de recherche français ou étrangers, des laboratoires publics ou privés.

19 **ABSTRACT**

20 Here we report a detailed characterization of the remodeling of photosynthesis upon sulfur
21 starvation under heterotrophy and photo-autotrophy in *Chlamydomonas reinhardtii*.
22 Photosynthetic inactivation under low light and darkness is achieved through specific
23 degradation of RuBisCO and cytochrome *b₆f* and occurs only in the presence of reduced
24 carbon in the medium. The process is likely regulated by nitric oxide (NO), which is
25 produced 24 hours after the onset of starvation, as detected with NO-sensitive
26 fluorescence probes visualized by fluorescence microscopy. We provide pharmacological
27 evidence that intracellular NO levels govern this degradation pathway: addition of a NO
28 scavenger decreases the rate of cytochrome *b₆f* and RuBisCO degradation while NO
29 donors accelerate the degradation. We have dissected the relative contribution of the
30 different NO synthesis pathways and we demonstrated that the NO₂-dependent NR-
31 independent pathway is crucial for NO production in these conditions. Our data argue for
32 an active role for NO in the remodeling of thylakoid protein complexes upon sulfur
33 starvation.

34

35 **INTRODUCTION**

36 In the wild, growth of photosynthetic autotrophs is often limited by nutrient availability.
37 Macronutrients as nitrogen, sulfur, phosphorus and carbon, the building bricks for all
38 biomolecules, are in suboptimal concentration in many ecosystems. Organisms have
39 evolved a variety of responses to adjust their metabolism to nutrient limitation, resulting in
40 their acclimation to environmental conditions. These responses can be divided into
41 general or nutrient-specific responses (Grossman, 2000; Merchant and Helmann, 2012;
42 Obata and Fernie, 2012). They comprise cell division arrest, changes in gene expression,
43 down regulation of anabolic pathways and up-regulation of catabolic pathways, activation
44 of scavenging processes and increased uptake from alternative sources. In several
45 instances, proteins rich in the lacking element are replaced by alternative isoforms with a
46 more appropriate amino acid composition.

47 In the green alga *Chlamydomonas reinhardtii*, the increasing number of available genetic
48 tools allows to study in more details ubiquitous and specific stress responses, such as
49 nutrient limitations (Grossman et al., 2007; Zhao et al., 2009; Schmollinger et al., 2013;
50 Sizova et al., 2013; Baek et al., 2016; Shin et al., 2016; Ferenczi et al., 2017; Greiner et
51 al., 2017; Baek et al., 2018). These stresses consistently encompass expression of
52 scavenging enzymes for the missing nutrient and selective degradation processes
53 (Merchant and Helmann, 2012; Saroussi et al., 2017). For instance, when facing
54 phosphorus starvation, *C. reinhardtii* attempts to recover phosphate by degrading a
55 fraction of the polyploid chloroplast chromosome and secreting phosphatases that
56 scavenge phosphate from the surrounding environment (Quisel et al., 1996; Wykoff et al.,
57 1998; Yehudai-Resheff et al., 2007). Phosphorus starvation also leads to an increased
58 susceptibility to photoinhibition, which targets primarily PSII (Quisel et al., 1996; Wykoff et
59 al., 1998; Malnoe et al., 2014).

60 Under nitrogen starvation, *C. reinhardtii* also degrades a fraction of its polyploid
61 chloroplast chromosome (Sears et al., 1980), while expressing an L-amino acid oxidase
62 (LAO1) as a scavenging enzyme in the periplasm **where it deaminates external amino**
63 **acids to release assimilable ammonium** (Vallon et al., 1993). In addition, cells undergo a
64 transition from a vegetative to a gamete state together with a replacement of their
65 ribosomes by other isoforms which are more error-prone (Picard-Bennoun and Bennoun,

66 1985; Bulte and Bennoun, 1990). Other changes upon nitrogen starvation encompass
67 storage of reduced carbon as starch and triacylglycerol lipids (TAGs) (Kajikawa et al.,
68 2015; Yang et al., 2015), and a block of photosynthesis due to a specific degradation of
69 cytochrome *b₆f* and RuBisCO (Bulte and Wollman, 1992; Wei et al., 2014).

70 **When starved for sulfur, *C. reinhardtii* down regulates dramatically global RNA translation**
71 **(Gonzalez-Ballester et al., 2010). To scavenge sulfur from external soluble sulfate esters**
72 **it synthesizes a periplasmic arylsulfatase (ARS) as a scavenging enzyme (Schreiner et**
73 **al., 1975).** It also accumulates TAGs, degrades sulfoquinovosyl diacylglycerol (SQDG)
74 (Sugimoto et al., 2007; Kajikawa et al., 2015; Yang et al., 2015) and down regulates
75 photosynthesis, a condition that can lead, under specific growth conditions, to hydrogen
76 evolution (Wykoff et al., 1998; Ghirardi et al., 2000; Melis et al., 2000; Zhang et al., 2002;
77 Antal et al., 2003; Forestier et al., 2003; Kosourov et al., 2003; Hemschemeier et al., 2008;
78 Grossman et al., 2011). However, there are conflicting reports as to the site at which
79 photosynthesis is actually inhibited upon sulfur starvation: it has been mainly attributed to
80 a PSII photodestruction (Wykoff et al., 1998; Nagy et al., 2016; Nagy et al., 2018) but
81 Malnoe et al. (2014) reported that this photoinhibitory effect was indirect, being the result
82 of a downstream block in photosynthetic electron transfer at the level of cytochrome *b₆f*
83 complexes. The selective degradation of cytochrome *b₆f* complex in absence of sulfur is
84 thus reminiscent of a similar process previously observed in absence of nitrogen sources
85 (Bulte and Wollman, 1992; Wei et al., 2014). These two macronutrients contribute to
86 widely different metabolic pathways that nevertheless overlap in some instances like the
87 biosynthesis of sulfur amino-acids or glutathione. In *C. reinhardtii*, sulfur assimilation is
88 regulated by the transmembrane polypeptide SAC1 (for sulfur acclimation 1), a
89 transporter-like protein induced upon sulfur limitation, and by the kinase SAC3, activated
90 through phosphorylation (Zhang et al., 2004; Pollock et al., 2005) **and involved in**
91 **transcriptional repression of cpRNA (Irihimovitch and Stern, 2006).** The sulfate anion
92 (SO_4^{2-}) is the preferred source of S and is imported by a number of transporters, some of
93 which, as SLT2, a sodium/sulfate co-transporter, are only expressed upon sulfur shortage.
94 Once inside, it must be activated by the enzyme ATP sulfurylase in order to be
95 assimilated. The activated form of SO_4^{2-} , Adenosine phosphosulfate (APS), can serve as
96 a substrate for SO_4^{2-} reduction or can be further phosphorylated by APS kinase to give 3'-

97 phosphoadenosine phosphosulfate (PAPS), used by sulfotransferases to catalyze the
98 sulfation of various cellular substrates (Pollock et al., 2005). In the pathway leading to
99 SO_4^{2-} reduction, the S of APS is reduced to SO_2^{2-} , which is further reduced to sulfide by
100 sulfite reductase in the chloroplast, with final incorporation into cysteine and methionine
101 (Leustek and Saito, 1999).

102 Given the similarities shared by nitrogen and sulfur starvation responses, it is tempting to
103 imagine that analogous signaling pathways are at work. The TOR signaling pathway was
104 recently discovered to play a major role in the response to starvation as a regulator of
105 S/C/N metabolism in plants (Dong et al., 2017) but other molecular players remain to be
106 discovered. Therefore, a deeper understanding of the mechanisms leading to
107 photosynthesis inactivation under sulfur starvation is required, notably the identification of
108 the signaling molecule(s) and of the metabolites from which they are produced.

109 Here, we characterized extensively the effects of sulfur starvation on the photosynthetic
110 apparatus of *C. reinhardtii*, using the same approaches and the same growth
111 (heterotrophy/photoautotrophy) and light conditions, that were previously used to study
112 nitrogen starvation (Wei et al., 2014). We aimed to gain information about the signal
113 involved in the remodeling of the photosynthetic apparatus and we found indeed many
114 similarities between sulfur and nitrogen limitations, providing evidence that NO plays a
115 key role also in the photosynthetic response to sulfur starvation.

116 **RESULTS**

117 **Sulfur starvation inactivates photosynthesis through specific degradation of** 118 **cytochrome *b₆f* and RuBisCO.**

119 Figure 1 shows the major photosynthetic changes undergone by the photosynthetic
120 apparatus of *C. reinhardtii* WT-S24⁻, a wild-type strain for photosynthesis, when starved in
121 sulfur for 72 hours under low light (5-15 $\mu\text{E}\cdot\text{m}^{-2}\cdot\text{sec}^{-1}$). When cells were starved for sulfur
122 in the absence of reduced carbon sources (M.M.-S), i.e. when survival strictly depends on
123 photosynthesis, the shape of the fluorescence transients remained indicative of an active
124 electron flow (Figure 1A right panel), with a limited decrease in Φ_{PSII} over 72 hours of
125 starvation (Figure 1B left panel). Despite a proper sensing of sulfur starvation, as

126 demonstrated by the induction of the SLT2 transporter (Figure 1C right panels), the
127 content in photosynthetic proteins showed no significant changes before 48h-72h of
128 starvation that caused some decrease in both cytochrome *b₆f* and RuBisCO.

129 In marked contrast, when kept in heterotrophic conditions, *Chlamydomonas* cells
130 displayed a dramatic decrease in electron transfer downstream of the plastoquinone pool
131 (Figure 1A left, grey line) but this was not due to PSII inactivation, as demonstrated by the
132 limited change in F_V/F_M (Figure 1B right, black line). Consistent with fluorescence data,
133 the content in PSII core proteins D1 and D2 only moderately decreased in these
134 experimental conditions (Figure 1C, left panels). By contrast, subunits from the
135 cytochrome *b₆f* complex and from RuBisCO became hardly detectable after 48 hours of
136 sulfur starvation, which identifies them as the main targets of photosynthesis inactivation
137 (see Supplemental Figure S1A for quantification). These findings correlate with
138 *Chlamydomonas* responses to nitrogen starvation (Wei et al., 2014) but also with previous
139 studies on *Dunaliella* (Giordano et al., 2000). Beside this marked inhibition in
140 photosynthesis, no major changes were observed for mitochondrial respiration
141 (Supplemental Figure S2A) while enhanced chlororespiration was observed with an
142 increased accumulation of the two major chlororespiratory enzymes NDA2 and PTOX2
143 (Figure 1C) concomitant with the augmented activity of the pathway (Supplemental Figure
144 S2B), as previously reported for cells starved in nitrogen (Wei et al., 2014).

145 The loss of cytochrome *b₆f* was consistent with the fluorescence induction kinetics typical
146 of a block of photosynthetic electron flow downstream of the plastoquinone pool (Figure
147 1A left, grey line), which explains the drop in Φ_{PSII} (Figure 1B left, black line). In an attempt
148 to better understand the mechanism of photosynthesis inhibition upon sulfur starvation,
149 we wondered whether cytochrome *b₆f* inactivation would occur first, then inducing its
150 degradation. We thus measured the peroxidase activity of the c-hemes which are
151 embedded within the cytochrome *b₆f* complex over the time of sulfur starvation. Using the
152 enhanced chemiluminescence method (Vargas et al., 1993) we observed that the loss of
153 the heme signals and the loss of their apoproteins followed similar kinetics (supplemental
154 Figure S1B), suggesting that protein degradation is not caused by heme inactivation.

155 The above results show a striking similarity with those obtained during nitrogen starvation
156 (Wei et al., 2014), where a similar remodeling of the photosynthetic apparatus was

157 observed. To further pursue the comparison between sulfur and nitrogen starvation, we
158 analyzed the impact of sulfur starvation in darkness and at higher light intensity, to
159 determine whether the remodeling of thylakoid proteins is induced by light and linked to
160 photo-damage events, or if it is a light-independent regulated process.

161 **The degradation of cytochrome *b₆f* and RuBisCO is light independent.**

162 Cells were starved for sulfur in heterotrophic medium (TAP-S), either in darkness or at
163 $120 \mu\text{E}\cdot\text{m}^{-2}\cdot\text{s}^{-1}$, an intensity often used to trigger sulfur starvation-induced hydrogen
164 production (Wykoff et al., 1998; Melis et al., 2000; Zhang et al., 2002; Antal et al., 2003;
165 Forestier et al., 2003; Hemschemeier et al., 2008; Nagy et al., 2016). Samples were
166 analyzed as above for fluorescence induction kinetics and by immunoblots (Figure 2). In
167 darkness, WT-S24⁻ exhibited responses similar to those observed under low light (Figure
168 1): Φ_{PSII} decreased dramatically with limited changes in F_V/F_M . Protein immune-detection
169 confirmed the specific degradation of cytochrome *b₆f* and RuBisCO (Figure 2C).

170 We noted that WT-S24⁻ better preserved PSII in darkness than another wild-type strain,
171 called T222⁺ (Malnoe et al., 2014). In the latter case there was a marked PSII inactivation
172 when S-starvation was performed in darkness (Supplemental Figure S3A). As shown by
173 the behavior of a representative tetrad of the progeny from a WT-S24⁻ x WT-T222⁺ cross,
174 there is indeed allelic variation between these two strains that nevertheless behave as
175 wild-type for photosynthesis in S-replete conditions (Supplemental Figure S3B).

176 By contrast with its behavior in darkness, WT-S24⁻ undergoing S-starvation at $120 \mu\text{E}\cdot\text{m}^{-2}\cdot\text{s}^{-1}$
177 showed an inhibition of photosynthesis due to photoinactivation of PSII, as indicated
178 by the decrease in F_V/F_M values (Figure 2B). Analysis of protein extracts demonstrates
179 that besides cytochrome *b₆f* and RuBisCO, PSI as well as PSII proteins also were
180 degraded at $120 \mu\text{E}\cdot\text{m}^{-2}\cdot\text{s}^{-1}$ (Figure 2C). Thus, upon sulfur starvation, high light induces
181 the degradation of several photosynthetic proteins, as reported in numerous former
182 studies (Wykoff et al., 1998; Antal et al., 2003), while under low light or darkness, a light-
183 independent mechanism targets cytochrome *b₆f* and RuBisCO and triggers thylakoid
184 remodeling in heterotrophic conditions.

185 **Specific degradation of cytochrome *b₆f* and Rubisco is controlled by chloroplast**
186 **proteases.**

187 To identify the mechanism of this selective protein loss, we investigated the role of the
188 two major proteases localized in the chloroplast and involved in abiotic stress responses,
189 ClpP (responsible for degradation of stromal proteins), and FtsH (involved in the
190 degradation of thylakoid membrane proteins) (Georgakopoulos et al., 2002; Sokolenko et
191 al., 2002). We first used the mutant *ftsh1-1*, which accumulates normal levels of an
192 inactive FtsH protease and is more sensitive to light, as demonstrated by its lower Φ_{PSII} in
193 S-replete conditions, compared to WT-S24⁻ (Malnoe et al., 2014) (Supplemental Figure
194 S4A). When starved of sulfur in heterotrophic conditions under low light, the *ftsh1-1* mutant
195 maintained cytochrome *b₆f* but still degraded RuBisCO, even though the cells were
196 struggling to find S, as demonstrated by the induction of the SLT2 transporter (Figure 3
197 left panels). Preservation of cytochrome *b₆f* is consistent with the very limited decrease in
198 Φ_{PSII} in the *ftsh1-1* mutant, where around 60% of the initial photosynthetic efficiency was
199 maintained after 72h (Supplemental Figure S4C). We then looked at the behavior of the
200 *clpP-AUU* mutant in similar conditions. *clpP-AUU* displays a four-fold reduced amount of the
201 Clp protease (Majeran et al., 2000) and has previously been demonstrated to respond
202 differently than WT-S24⁻ to N-starvation (Wei et al., 2014). In this mutant cytochrome *b₆f*
203 was still degraded, albeit at a lower rate, while RuBisCO remained unaltered. We noted
204 that PSII and ATP synthase were targeted to degradation at a later stage of starvation
205 which is indicative of an enhanced susceptibility of the cells to the absence of sulfur when
206 the activity of ClpP is hampered.

207 Altogether these experiments show that, in the absence of sulfur, degradation of stromal
208 RuBisCO is under the control of the stromal Clp protease whereas degradation of the
209 integral cytochrome *b₆f* complex is under the control of the transmembrane FtsH protease.
210 The preserved accumulation of the cytochrome *b₆f* complex and of RuBisCO in the
211 proteases mutant strains also excluded a significant contribution of transcriptional and
212 translational regulation to the remodeling of the photosynthetic apparatus in our
213 experimental conditions.

214 **Sustained production of nitric oxide occurs under sulfur starvation**

215 We have previously shown that nitric oxide (NO) is produced when *C. reinhardtii* is starved
216 in nitrogen (Wei et al., 2014). NO is produced in a series of abiotic stresses during which
217 it is suspected to act as a signaling molecule that modulates enzymatic activities, protein
218 localization and proteolytic susceptibility (Wendehenne and Hancock, 2011; Zaffagnini et
219 al., 2016; Blaby-Haas and Merchant, 2017). Although NO production in *C. reinhardtii*
220 under sulfur starvation has recently been documented (Minaeva et al., 2017), the kinetics
221 of synthesis and the source(s) of this molecule are still to be elucidated. Thus we sought
222 to better characterize NO production sources and NO effects under sulfur limitation using
223 a fluorescence microscopy approach. To detect endogenous NO production *in situ*, we
224 monitored fluorescence levels after incubation with the NO-specific fluorescent probe 4-
225 amino-5-methylamino-2',7'-difluoro-fluorescein diacetate (DAF-FM DA). This permeant
226 molecule is naturally non-fluorescent. After entering the cell it get esterified, becomes non-
227 permeant, and remains trapped inside the cell. In the presence of NO (or of its oxidation
228 products N_2O_3 and NO^+), it is converted into the highly fluorescent triazol derivative.
229 To observe NO production, WT-S24⁻ cells were starved of sulfur and, at indicated time
230 points, aliquots were harvested, incubated for 1 hour in the presence of DAF-FM DA (5
231 μ M) before recording fluorescence levels. Figure 4 shows chlorophyll auto-fluorescence
232 in red and the DAF-FM DA signal in green. In cells kept in TAP medium the green
233 fluorescence was not observed but only the red signal in the chloroplasts (Supplemental
234 Figure S4, left panels). When cells were incubated with DEA NONOate (a strong NO-
235 donor), the signal of DAF-FM DA increased strongly, especially in **extra-chloroplastic**
236 **compartments** (Supplemental Figure S5, middle panels). When cells were transferred in
237 TAP-S medium, a faint-green signal appeared after 12-15 hours (data not shown), and
238 became prominent after 24 hours of starvation (Figure 4). It then remained at a high level
239 for the whole duration of the experiment, with a fluorescence emission originating from **all**
240 **compartments**. This signal disappears when the NO-scavenger Carboxy-PTIO potassium
241 salt (cPTIO), highly efficient for NO removal, was added to the starvation medium,
242 demonstrating that it actually originates from NO (Supplemental Figure S5, right panel).
243 Chlorophyll fluorescence parameters were also measured in parallel and we observed
244 that NO production starts together with the steep drop in Φ_{PSII} (data not shown). Thus

245 sulfur starvation leads to a sustained NO production over four days, concomitant with
246 cytochrome *b₆f* and RuBisCO degradation.

247 Since the response to sulfur starvation depends on growth conditions, we repeated the
248 same NO measurements in phototrophic conditions (M.M.-S, Figure 5) that lead to a
249 limited decrease in the quantum yield of fluorescence. In these conditions we only
250 observed a faint green fluorescence emission, indicating that NO was not significantly
251 produced. Thus, the absence of cytochrome *b₆f* and RuBisCO degradation correlates with
252 the absence of NO production.

253 These observations constitute a first indication that NO, whose production is subordinated
254 to growth conditions, is involved in the response to sulfur limitation in *C. reinhardtii*. In
255 order to get further insights into the link between NO production and the remodeling of the
256 photosynthetic apparatus, we designed a series of experiments using diverse NO donors
257 and scavengers.

258 **Testing the involvement of nitric oxide as a triggering signal.**

259 To understand whether NO plays a direct role in the remodeling of the photosynthetic
260 apparatus, we modulated its intracellular concentration using pharmacological
261 approaches. We starved WT-S24⁻ cells in TAP-S at 15 $\mu\text{E m}^{-2} \text{s}^{-1}$ for 24 hours before
262 adding NO-donors possessing different NO-release kinetics: sodium nitroprusside (SNP)
263 and S-Nitroso-N-acetyl-DL-penicillamine (SNAP). In parallel we tested the NO-scavenger
264 cPTIO. Donors were added either alone or in the presence of cPTIO to verify possible
265 indirect effects not related to NO (Figure 6 and Supplemental Figure S6). After drug
266 addition, photosynthetic efficiency and protein accumulation were analyzed during 8
267 hours, in comparison to untreated control, WT-S24⁻ in TAP-S. Donors and scavengers
268 were added 24 h after the onset of starvation, when photosynthetic parameters start to
269 change significantly (Figure 1B).

270 The results, shown in Figure 6, demonstrate that the amount of intracellular NO affects
271 photosynthetic efficiency during S-starvation. All drugs had a significant impact on
272 photosynthesis and acted downstream of PSII, as indicated by the limited effects on F_v/F_M
273 (Figure 6A).

274 Addition of cPTIO alone during S starvation largely slowed down photosynthesis inhibition
275 (Figure 6A, squares) and this effect was also observed when cPTIO was added every 24
276 hour for the entire duration of the starvation (Supplemental Figure S6A). Removing
277 endogenous NO preserves photosynthetic efficiency, probably by blocking the signal that
278 triggers protein degradation. Indeed, when analyzing by immunoblot the content in
279 cytochrome *f* and RuBisCO at the onset of starvation (0 h), before (24 h) and after (32 h)
280 incubation with cPTIO (0.2 mM), we clearly observed that cytochrome *f* and RuBisCO
281 degradation was prevented (Figure 6B, left panels). Strikingly, after 8 hours of cPTIO
282 treatment protein levels were higher than at the time of addition (24 h) (Figure 6C for
283 quantification). Moreover, D1 accumulation appeared unchanged by NO levels,
284 suggesting again that the specific degradation of cytochrome *b₆f* and RuBisCO is
285 regulated independently, at least in these conditions.

286 Addition of SNP and SNAP both caused a more pronounced and faster decrease in
287 quantum yield (Figure 6A, triangles and stars). The stimulated inhibition of photosynthesis
288 by these NO donors was fully counteracted by cPTIO when added concomitantly
289 (Supplemental Figure S6 B-C), suggesting that the observed effect was likely due to NO
290 accumulation rather than to unspecific effects of these drugs. The faster inhibition of
291 photosynthesis does correlate with faster protein degradation even though the effects
292 observed in these cases were stronger for cytochrome *b₆f* than for RuBisCO. The
293 quantification of RbcL indeed did not show strong differences between treated and non-
294 treated samples (Figure 6B-C). Nevertheless, both donors were found to accelerate the
295 degradation of cytochrome *b₆f* with a more prominent effect for SNP.

296 Together, our data indicate that cPTIO-dependent scavenging of endogenous NO blocks
297 protein degradation and preserves photosynthetic efficiency, while exogenous addition of
298 NO accelerates the degradation process and inactivates photosynthesis much faster.
299 These results strongly suggest that NO is a key signaling molecule for photosynthetic
300 inactivation under sulfur starvation.

301

302 **The source of NO**

303 That NO is crucial for photosynthetic regulation raises the question of its source upon S-
304 starvation. To address this point, we used a series of distinct NO synthesis inhibitors.
305 WT-S24⁻ is a strain which lacks nitrate reductase (NR) (*nit1-137 nit2-124 mt2*), an enzyme
306 involved in NO production (Sakihama et al., 2002; Chamizo-Ampudia et al., 2016). Thus,
307 we chose specific inhibitors of the NR-independent NO-producing pathways, We used L-
308 N^G-Nitroarginine methyl ester (L-NAME) and Amino guanidine (AG) to block the NOS-like
309 dependent pathway, DL- α -Difluoromethylornithine (DFMO) to block the polyamine-
310 dependent pathway and tungstate to block the synthesis of MoCo, a molybdenum cofactor
311 required for the activity of 5 enzymes (nitrate reductase; sulfite reductase; xanthine
312 oxido/reductase, aldehyde dehydrogenase and the Amidoxine Reducing Component,
313 ARC, recently renamed NO-forming Nitrite Reductase or NOFNIR) all of which have been
314 described as putative Nitrite-dependent producers of NO (Tewari et al., 2009; Wang et al.,
315 2010; Maia and Moura, 2011; Wei et al., 2014; Chamizo-Ampudia et al., 2016). We added
316 these inhibitors twice, every 24 hours, to reach a 1 mM final concentration at the end of
317 the experiment. These drugs had no significant effect in control cultures kept in TAP
318 (Supplemental Figure S7B). By contrast, when WT-S24⁻ cells were starved in TAP-S, all
319 inhibitors slowed down the inhibition of photosynthesis (Figure 7). These results clearly
320 demonstrate that all pathways are involved in the production of NO upon sulfur starvation.
321 Indeed L-NAME, AG, DFMO and Tungstate all preserved photosynthetic efficiency
322 although to a different extent. Interestingly, tungstate was the most effective in preserving
323 photosynthesis, suggesting a prominent role of Nitrite-dependent pathways, even in the
324 absence of the NR enzyme.

325 **DISCUSSION**

326 When starved for sulfur, *C. reinhardtii* slowly undergoes photosynthesis inactivation,
327 which is completed within four days. This functional inhibition is achieved through the
328 specific degradation of RuBisCO and cytochrome *b₆f*, respectively controlled by the
329 stromal and thylakoid proteases ClpP and FtsH. Our data are in contrast with previous
330 studies on sulfur starvation, most of which have described a photosynthetic inhibition due
331 to PSII inactivation/degradation (Wykoff et al., 1998; Grossman, 2000; Zhang et al., 2002;
332 Forestier et al., 2003; Zhang et al., 2004; Nagy et al., 2016; Nagy et al., 2018). These

333 studies focused on H₂ production which requires higher light intensities during starvation
334 (80-300 μE·m⁻²·s⁻¹) than those we used to observe the selective degradation of
335 cytochrome *b₆f* and RuBisCO. Indeed, we have shown previously (Malnoe et al., 2014),
336 and confirmed here, that increasing the light intensity at which S-starvation is performed
337 triggers photoinhibitory processes which drive inactivation and degradation of PSII, and
338 also PSI. This is a straightforward consequence of the lower metabolic demand for carbon
339 fixation upon growth arrest, which leads to NADPH accumulation, over-reduction of the
340 photosynthetic electron transfer chain and ROS production which will damage PSI and
341 PSII. The decreased pool of sulfur amino-acids should also contribute to photoinhibition
342 by slowing down protein synthesis, thus repair cycles.

343

344 *Physiological responses to nutrient starvation*

345 The light-independent degradation of RuBisCO when *C. reinhardtii* is starved for sulfur
346 can be viewed as an attempt to remobilize sulfur. Indeed, RuBisCO, the most abundant
347 protein on Earth that amounts to about 30% of the soluble proteins in *C. reinhardtii*
348 (Sugimoto et al., 2007; Michelet et al., 2013), is a major reservoir of sulfur. Being
349 composed of 8 large and 8 small subunits that together contain 256 sulfur atoms
350 embedded in cysteine or methionine residues, its degradation would allow the cells to
351 cope with a transient decrease in external sulfur sources.

352 Sulfur remobilization is not likely to explain degradation of cytochrome *b₆f* which, despite
353 its 27 methionines, 13 cysteines, and a [2Fe-2S] prosthetic group per monomer (Stroebel
354 et al., 2003), is not a major source of sulfur compared to other photosynthetic protein
355 complexes such as PSII (86 sulfur-containing residues in the core subunits) and PSI (80
356 sulfur-containing residues and 4 [4Fe-4S] clusters in the core subunits). Its degradation
357 rather should be taken as indicative of a response aimed at preventing photosynthetic
358 electron transfer upon growth arrest.

359 The dual-targeted degradation of RuBisCO and cytochrome *b₆f* in sulfur-deprived
360 conditions is better understood when compared with the very similar situation produced
361 by nitrogen deprivation (Wei et al., 2014). In both conditions, the central metabolism slows
362 down drastically, leading to growth arrest and down regulation of gene expression. Thus,
363 the energy demand for DNA replication, translation and protein synthesis dramatically

364 decreases. At the same time, catabolic pathways are activated to remobilize as much
365 sulfur or nitrogen as possible. Up-regulation of catabolism leads to over accumulation of
366 reduced carbon, mainly as starch and TAG lipids (Kajikawa et al., 2015). Since carbon
367 metabolism is intimately linked to nitrogen and sulfur metabolism, with which it shares a
368 mutual genetic regulation (Kopriva and Rennenberg, 2004), the cells would try to avoid
369 such imbalance between these macronutrients, by shifting, in heterotrophic conditions,
370 toward respiration at the expense of photosynthesis: RuBisCO degradation prevents
371 carbon assimilation and thus over-accumulation of additional carbon skeletons whereas
372 cytochrome *b₆f* degradation blocks altogether the cyclic and linear electron flows, thus
373 collapsing photosynthetic ATP and NADPH production. Mitochondrial respiration will
374 provide enough energy to sustain the limited cell metabolism, and consume at the same
375 time the carbon skeletons in excess. It is also of note that chlororespiration is stimulated
376 upon sulfur deprivation, as it is upon nitrogen starvation (Wei et al., 2014). Thus the
377 chloroplast becomes a catabolic organelle to balance C, N and S levels in coordination
378 with mitochondria. These responses to N and S deprivation are activated in heterotrophic
379 conditions but not in phototrophic conditions. This contrast calls for responses to
380 starvation through a hierarchy of signals, the first one being the availability of reduced
381 carbon in the medium. Its presence allows a sustained respiratory metabolism which
382 should trigger the switch toward photosynthesis inactivation when the signal “sulfur or
383 nitrogen deprivation” is perceived. This is consistent with the absence of photosynthesis
384 inactivation when *C. reinhardtii* is starved for nitrogen in the absence of mitochondrial
385 respiration (Bulte and Wollman, 1990; Wei et al., 2014). This situation, similar to the
386 absence of external reduced carbon sources (photoautotrophic conditions), does not lead
387 to degradation of RuBisCO and cytochrome *b₆f*, and preserves photosynthesis until the
388 internal S and N resources are completely exhausted.

389

390 *NO as a key factor for metabolic response to nutrient deprivation*

391 A key element in photosynthesis inactivation upon N or S deprivation is the accumulation
392 of NO, which is instrumental in the degradation of cytochrome *b₆f* and RuBisCO (Wei et
393 al. 2014 and this study). Its strong accumulation could result either from its increased
394 production or from a decreased efficiency of NO-scavenging systems in the chloroplast.

395 The latter process may be borne by flavodiiron proteins at the acceptor side of PSI. These
396 proteins, called FLVA and FLVB in *Chlamydomonas*, have been ascribed a role in
397 ROS/RNS detoxification in bacteria and archea (Chaux et al., 2017). They assemble into
398 heterodimers that would play a role in acclimation to fluctuating light (Zhang et al., 2009;
399 Jokel et al., 2015; Gerotto et al., 2016; Saroussi et al., 2017). Interestingly, upon sulfur
400 deprivation FLVA/FLVB are initially induced within the first 24 hours and subsequently
401 degraded (Jokel et al., 2015). The kinetics of this degradation fit perfectly with our results
402 and may suggest that flavodiiron degradation enhances NO accumulation under sulfur
403 starvation.

404 That an increased production of NO also plays a role in the present protein degradation
405 process, is supported by our experiments with NO-scavengers, supporting its direct
406 involvement in the degradation process. In *Chlamydomonas* two major NO synthesis
407 pathways have been described. The main one is the Nitrite-dependent pathway, involving
408 either nitrate reductase (NR) and the ARC enzyme (Chamizo-Ampudia et al., 2016), or an
409 NR-independent process still to be characterized at the molecular level (Hemschemeier
410 et al., 2013; Wei et al., 2014). The other pathway is the arginine dependent pathway,
411 occurring either from the degradation of polyamines or through an as yet unidentified
412 NOS-like enzyme (Barroso et al., 1999; Corpas et al., 2004; Tun et al., 2006; Yamasaki
413 and Cohen, 2006). Here, using various inhibitors of NO synthesis we provided evidence
414 that the NR-independent Nitrite-dependent pathway plays a major role upon sulfur
415 deprivation.

416 Two possible mechanisms for the NO-stimulated protein degradation may come into play.
417 NO could induce redox post-translational modifications such as nitrosylation (Astier and
418 Lindermayr, 2012; Morisse et al., 2014; Zaffagnini et al., 2016) or tyrosine nitration
419 (Jacques et al., 2013; Mata-Perez et al., 2016), which may target proteins for degradation
420 or modify the proteases responsible for degradation, thus acting either as a tag or a
421 trigger. Alternatively, it may affect NO-responsive enzymes like guanylate cyclase and
422 truncated hemoglobins, which would then activate even more complex signaling pathways
423 to reach acclimation. Recently, the truncated hemoglobin THB1 was shown to be induced
424 upon sulfur starvation and to be involved in NO detoxification, while controlling the
425 expression of some sulfur-responsive genes. (Minaeva et al., 2017). Indeed, NO can fulfill

426 a signaling function either in couple with hemoglobins, after direct interaction with heme
427 groups (Ouellet et al., 2002; Perazzolli et al., 2004; Perazzolli et al., 2006; Smaghe et
428 al., 2008; Hemschemeier et al., 2013; Minaeva et al., 2017), or as a nitrosylating agent
429 coupled with GSH or with other proteins considered as alternative nitrosylases (Kornberg
430 et al., 2010; Stamler and Hess, 2010; Nakamura and Lipton, 2013; Zaffagnini et al., 2013;
431 Zaffagnini et al., 2016). In that respect, glutathione, a cysteine-containing tripeptide, may
432 be crucial for the diffusion of the signal.

433 Glutathione is the main redox buffer, a key molecule at the crossroad between carbon,
434 nitrogen and sulfur metabolisms, playing a major role in stress responses, NO metabolism
435 and signaling. Reduced glutathione (GSH) is the main denitrosylating molecule for most
436 nitrosylated proteins. It also interacts with NO to form the GSNO molecule, the main NO
437 reservoir of the cell and the main transnitrosylating agent. . Therefore the GSH/GSNO
438 ratio critically controls nitrosylation levels (Zaffagnini et al., 2013). In Chlamydomonas, the
439 glutathione content strongly decreases during sulfur starvation either in autotrophy (Fang
440 et al., 2014) or in mixotrophy (Supplemental Figure S8).The breakdown of glutathione
441 may facilitate ROS-induced over-oxidation and nitrosative stress, two events which are
442 enhanced under sulfur deprivation, where the Calvin-Benson cycle is blocked and the
443 photosynthetic electron transfer chain becomes over-reduced. The decreased content of
444 glutathione under sulfur starvation may therefore contribute to reinforce the signaling
445 triggered by NO.

446 As to the high specificity of the nitrosylation-based signal it is of note that alternative
447 nitrosylases, when nitrosylated are able to transfer their NO moiety to downstream targets,
448 with a high degree of specificity. Only few trans-nitrosylases have been described in the
449 literature including -SNO-hemoglobin, SNO-glyceraldehyde-3-phosphate
450 dehydrogenase, SNO-caspase 3 and SNO-Thioredoxin 1 (Kornberg et al., 2010; Stamler
451 and Hess, 2010; Nakamura and Lipton, 2013; Zaffagnini et al., 2016) none of them in
452 photosynthetic organisms. Theoretically, transnitrosylation may lead to the nitrosylation of
453 proteins that are not themselves target of direct nitrosylation by NO or related molecules
454 like GSNO, thereby amplifying the signal. The signaling pathway could therefore be a
455 multi-step cascade, with increased specificity at each step, starting from the highly
456 reactive and poorly specific NO to end up with highly specific nitrosylases. In

457 photosynthetic organisms, nitric oxide, besides its involvement in physiological responses
458 (Beligni and Lamattina, 2000; Neill et al., 2002; Pagnussat et al., 2002; He et al., 2004;
459 Prado et al., 2004; Mishina et al., 2007; Tada et al., 2008; Lindermayr et al., 2010; Gibbs
460 et al., 2014), is also implicated, in many stress responses with increased oxidative load
461 (Delledonne et al., 1998; Garcia-Mata and Lamattina, 2001; Graziano et al., 2002;
462 Feechan et al., 2005; Baudouin et al., 2006; Zhao et al., 2007; Lee et al., 2008; Lee et al.,
463 2008; Besson-Bard et al., 2009; Blaby-Haas and Merchant, 2017), among which nitrogen
464 starvation (Wei et al., 2014).

465

466

467 **METHODS**

468 **Strains, Media, Culture conditions, Chemicals**

469 *C. reinhardtii* wild-type S24⁻ (CC-5100, (Gallaher et al., 2015), *ftsH1-1* (Malnoe et al.,
470 2014) and *clpP_{AUU}* (Majeran et al., 2000) were grown on a shaker at 140 rpm, under
471 continuous light (5 to 15 $\mu\text{E}\cdot\text{m}^{-2}\cdot\text{s}^{-1}$ for low light; 120 $\mu\text{E}\cdot\text{m}^{-2}\cdot\text{s}^{-1}$ for high light), or in
472 darkness, at 25°C. For sulfur starvation experiments, cells were pregrown in TAP (Tris-
473 acetate-phosphate) medium (pH 7.2) (Harris, 1989) under continuous light (5 to 15 $\mu\text{E}\cdot\text{m}^{-2}\cdot\text{s}^{-1}$)
474 to reach a concentration of 2×10^6 cells $\cdot\text{mL}^{-1}$ (mid log phase). Cells were then
475 centrifuged at 3000g for 5 min at room temperature, washed once in sulfur-free medium,
476 resuspended at 2×10^6 cells $\cdot\text{mL}^{-1}$ in sulfur-free medium provided (TAP) or not (Minimum
477 Medium) with acetate (respectively named TAP-S and M.M.-S), and kept on a rotary
478 shaker with vigorous aeration (210 rpm). Carboxy-PTIO potassium salt (cPTIO); sodium
479 nitroprusside (SNP), S-Nitroso-N-acetyl-DL-penicillamine (SNAP), Diethylamine
480 NONOate diethylammonium salt (DEA NONOate), 4-amino-5-methylamino-2',7'-difluoro-
481 fluorescein diacetate (DAF-FM DA), DL- α -Difluoromethylornithine hydrochloride (DFMO),
482 N ω -Nitro-L-arginine methyl ester (L-NAME), Amino guanidine (AG) and Tungstate were
483 all purchased from Sigma-Aldrich®. Fresh solutions were prepared before each
484 experiment and were kept on ice and in darkness for no longer than 6 hours.

485 **Protein Preparation, separation and analysis**

486 Protein extraction and immunoblot analyses were performed as described in (Kuras and
487 Wollman, 1994). Cell extracts were loaded on an equal chlorophyll basis (3.5 μg per lane).
488 Chlorophyll quantification was performed by measuring absorbance of SDS solubilized
489 samples at 680 nm, where, after a 200-fold dilution, $\text{Abs}_{680}=0.11$ corresponds to 1 $\mu\text{g}\cdot\mu\text{L}^{-1}$
490 of Chl in the sample. For each experiment shown, at least three biological replicates
491 were analyzed. Each sample was loaded on mirror gels and best representative blots are
492 shown in figures. All raw images used to prepare composite figures are included in a
493 compressed file (Supplemental dataset 1). Protein detection was performed with ECL
494 (Pierce®) in a Chemidoc™ XRS+ System scan for membranes (BioRad®). Band
495 quantification was done using the ImageLab (v.3.0) software. Primary antibodies were

496 diluted as in (Wei et al., 2014) and (Malnoe et al., 2014). All antibodies were revealed by
497 horseradish peroxidase-conjugated antibody against rabbit IgG (Promega®). Antibodies
498 against D1, D2, PsaA, SLT2, and LHCII were purchased from Agrisera®. RuBisCO
499 antibodies were kindly provided by the group of S. Whitney, Australia. Other antibodies
500 were described previously: cytochrome *b₆f* subunits (Kuras and Wollman, 1994), β subunit
501 of ATP-synthase (Drapier et al., 1992), PTOX2 (Houille-Vernes et al., 2011), NDA2
502 (Desplats et al., 2009).

503 **Detection of c-type Hemes using the ECL western blotting detection reagents**

504 ECL (Pierce®) reagents were used as in (Vargas et al., 1993) according to the
505 manufacturers' recommendations (Pierce®). The detection solution was added directly
506 on the membrane surface after the transfer and incubated for 1 min. After draining the
507 excess of solution, membranes were revealed using the Chemidoc™ XRS+ System scan
508 for membranes (BioRad®). Experiments were repeated at least three times
509 independently.

510 **Fluorescence Measurements**

511 Liquid cultures were dark-adapted under strong agitation for 30 min in open Erlenmeyer
512 flasks and fluorescence was then recorded using a home-built fluorimeter. Measurements
513 were carried out for a time-span of 2.5 s, with a final pulse of saturating actinic light. The
514 following parameters were recorded: F_0 , fluorescence yield of dark adapted cells; F_M , the
515 fluorescence yield of the same cells after the saturating actinic pulse; F_S , the steady state
516 fluorescence yield reached under a continuous illumination ($250 \mu\text{E}\cdot\text{m}^{-2}\cdot\text{s}^{-1}$), recorded
517 before the saturating light pulse. Quantum yield and F_V/F_M were calculated as follows:
518 $\Phi_{\text{PSII}} = (F_M - F_S)/F_M$; $F_V/F_M = (F_M - F_0)/F_M$.

519 **Fluorescence Microscopy**

520 Aliquots (15 mL) of cultures starved for the indicated times, were incubated 1 h in the
521 presence of $5 \mu\text{M}$ DAF-FM DA, washed and concentrated 10 times by centrifugation at
522 $3000 g$, 5 min, at RT, in sulfur-depleted medium and imaged rapidly at room temperature
523 with a Zeiss® Axio Observer Z1 microscope equipped with a PA 63x/1.4 oil objective.

524 Excitation was performed simultaneously for Chlorophyll and DAF-FM DA using a blue
525 led coupled with a cut-off filter at 470 nm. Emission was recorded separately for DAF-FM
526 DA (595 nm) and chlorophyll (650 nm), in order to separate the signals arising from the
527 NO sensor or from endogenous chlorophyll. Images were obtained either with single
528 pictures or with 2 x 2 tile scanning. Images were collected and treated with the ZEN 2011
529 (Zeiss®) software. The specificity of DAF-FM for NO was tested using DEA NONOate and
530 cPTIO.

531 **NO donors and NO-scavengers**

532 WT-S24⁻ cells (150 mL), at a concentration of 2×10^6 cells·mL⁻¹, were transferred in Sulfur-
533 free medium (TAP-S) for 24 h in a 500 mL Erlenmeyer flask. Equal volumes of the original
534 culture were divided in 250 mL Erlenmeyer flasks, one flask for each incubation (namely
535 control; cPTIO; SNP; SNAP; SNP + cPTIO; SNAP + cPTIO). Drugs were added
536 immediately after sampling (T24) at the following concentrations: cPTIO 0.2 mM; SNP 0.5
537 mM; SNAP 0.5 mM; the same concentrations were used when different drugs were added
538 simultaneously in mixtures. Samples were taken every 2 hours, then dark-adapted under
539 strong agitation for 30 min in open Erlenmeyer flasks. Photosynthetic parameters were
540 calculated from the fluorescence records as described above (see Fluorescence
541 measurements).

542 **NO-synthesis inhibitors**

543 Treatment of WT-S24⁻ cells starved in sulfur, was as above. A series of 250 mL
544 Erlenmeyer flasks, encompassed a control; L-N^G-Nitroarginine methyl ester (L-NAME);
545 Amino guanidine (AG); DL- α -Difluoromethylornithine (DFMO); tungstate. Drugs were
546 added immediately after the first sampling (T24) and after one day (T48), to reach a final
547 concentration of 1 mM for each compound. Fluorescence parameters were recorded as
548 described above.

549 **ACKNOWLEDGMENTS**

550 The authors thank Sandrine Bujaldon and Clara Ameller for technical assistance, Dr
551 Stefania Viola for help in measurements of chlororespiration rates, Dr Zhou Xu for help

552 during microscopy analyses and Catherine de Vitry for many stimulating discussions and
553 suggestions. This work was supported by the CNRS and Sorbonne University and by
554 LABEX DYNAMO ANR-LABX-011.

555 **FIGURE LEGENDS**

556 **Figure 1. Effects of sulfur deprivation on the photosynthetic apparatus in different**
557 **growth conditions.**

558 **(A)** Kinetics of fluorescence induction of dark adapted (30 min) WT-S24⁻ cells in TAP-S
559 and M.M.-S, recorded at t_0 and t_{72} . a.u. = arbitrary units.

560 **(B) LEFT** Φ_{PSII} (quantum yield) calculated as $(F_M - F_S) / F_M$. This parameter shows the
561 efficiency of the entire electron transport chain. **RIGHT** F_V / F_M calculated as $(F_M - F_0) / F_M$.
562 This parameter gives information about the PSII efficiency. Black line (squares): TAP-S
563 (with acetate); gray line (circles): M.M.-S (without acetate). Mean of seven independent
564 experiments \pm SEM.

565 **(C)** Whole protein extracts of cells harvested at indicated time points after the onset of
566 sulfur starvation, probed with the indicated antibodies. β -CF₁ and LHCII are internal
567 loading controls. Each condition was analyzed at least thrice. To detect all proteins,
568 samples from each replicate were loaded on mirror gels. Best representative blots are
569 shown. Left panel shows protein levels of cells starved in TAP-S, right panel shows protein
570 levels of cells starved in M.M.-S.

571 **Figure 2. Effects of sulfur deprivation in darkness and at 120 μ E m⁻² s⁻¹.**

572 **(A), (B)** Evolution of Φ_{PSII} and F_V / F_M of WT-S24⁻ starved in TAP-S. Black line (squares):
573 complete dark; dashed line (triangles): High Light 120 μ E m⁻² s⁻¹. Data represent the mean
574 of 3 experiments \pm SEM.

575 **(C)** Whole protein extracts from High Light samples (left panels) and dark samples (right
576 panels), harvested at indicated time points and probed with indicated antibodies. β -CF₁ is
577 an internal loading control. Each condition was analyzed at least thrice. To detect all
578 proteins, samples from each replicate were loaded on mirror gels. Best representative
579 blots are shown.

580 **Figure 3. Sulfur starvation in *ftsh1-1* and *clpP_{AUU}* mutants**

581 Whole protein extracts from cells starved in TAP-S at $15 \mu\text{E m}^{-2} \text{s}^{-1}$, harvested at indicated
582 time points and probed with indicated antibodies. $\beta\text{-CF}_1$ is an internal loading control. Each
583 mutant was analyzed at least thrice. To detect all proteins, samples from each replicate
584 were loaded on mirror gels. Best representative blots are shown.

585 **Figure 4. Nitric oxide production during sulfur starvation in heterotrophic growth**
586 **conditions.**

587 Visualization of NO production *in vivo*, using the DAF-FM DA ($5 \mu\text{M}$) probe. WT-S24⁻ cells
588 were starved in TAP-S at $15 \mu\text{E m}^{-2} \text{s}^{-1}$, harvested at indicated time points and observed
589 with a fluorescence microscope after a washing step in sulfur free medium and 10-fold
590 concentration. CHLORO, chlorophyll autofluorescence; DAF-FM DA, NO-dependent
591 green fluorescence; MERGE, chlorophyll and NO-dependent signals visualized together.

592 **Figure 5. Nitric oxide production during sulfur starvation in photo-autotrophic**
593 **growth conditions.**

594 Visualization of NO production *in vivo*, using the DAF-FM DA ($5 \mu\text{M}$) probe. WT-S24⁻ cells
595 were starved in M.M.-S at $15 \mu\text{E m}^{-2} \text{s}^{-1}$, harvested at indicated time points and observed
596 as in Figure 4.

597 **Figure 6. Nitric oxide accumulation affects the kinetics of photosynthesis inhibition**
598 **and cytochrome *b6f* degradation.**

599 **(A)** Photosynthetic parameters evolution, Φ_{PSII} (left) and F_v/F_m (right), measured after
600 addition (indicated by arrows) of NO-donors (SNAP 0.05 mM and SNP 0.5 mM) or NO-
601 scavenger (cPTIO 0.2 mM) on WT-S24⁻ cell starved in TAP-S medium at $15 \mu\text{E} \cdot \text{m}^{-2} \text{s}^{-1}$;
602 dashed line corresponds to the control (cells in TAP-S without any drug addition). Data
603 show the mean of five independent experiments \pm SEM. Statistical significance was
604 assessed using 2 way ANOVA test ($P < 0.05$) between control (non-treated) and drug-
605 treated samples. SNP, SNAP and cPTIO score with $P < 0.01$.

606 **(B)** Immunoblots showing the accumulation of indicated proteins. Extraction were
607 performed before and after drug addition (cPTIO 0.2 mM; SNP 0.5 mM; SNAP 0.05 mM)
608 during starvation in TAP-S at $15 \mu\text{E} \cdot \text{m}^{-2} \cdot \text{s}^{-1}$. $\beta\text{-CF}_1$ is an internal loading control. Each

609 condition was analyzed at least thrice. To detect all proteins, samples from each replicate
610 were loaded on mirror gels. Best representative blots are shown.

611 **(C)** Relative band intensity \pm SEM for Cyt *f* and RbcL before and after cPTIO 0.2 mM,
612 SNP 0.5 mM, SNAP 0.05 mM treatments. Data are normalized to T_0 . Stars correspond to
613 significant differences assessed with 1 way ANOVA test ($P < 0.05$). cPTIO $P = 0.03$ and
614 $P = 0.015$ for cyt *f* and RbcL respectively; SNP $P = 0.031$ for cyt *f*.

615 **Figure 7. Effects of different NO-synthesis inhibitors on photosynthetic efficiency.**

616 Photosynthetic parameters evolution, Φ_{PSII} (top) and F_v/F_m (bottom), measured after
617 addition (indicated by arrows) of L-NAME (1 mM); DFMO (1 mM); Tungstate (1 mM),
618 Amino guanidine (AG) (1 mM) on WT-S24⁻ cells starved in TAP-S at $15 \mu E \cdot m^{-2} \cdot s^{-1}$. Black
619 line (diamonds) corresponds to the control (cells in TAP-S without any drug addition). Data
620 show the mean of four independent experiments \pm SEM. Statistical significance was
621 assessed using 2 way ANOVA test ($P < 0.05$) between control (non-treated) and inhibitor-
622 treated samples. All drugs show a score of $P < 0.01$.

623 **Fig. S1. Photosynthetic complex accumulation upon sulfur starvation and** 624 **correlation between cytochrome *b6f* degradation and inactivation.**

625 **(A)** Relative band intensity of indicated antibodies for WT-S24⁻ cells starved in TAP-S
626 medium at $15 \mu E m^{-2} s^{-1}$. Data show the mean of three independent experiments \pm SEM,
627 values are normalized to 100% for T_0 .

628 **(B)** Whole protein extracts from WT-S24⁻ cells starved in TAP-S at $15 \mu E m^{-2} s^{-1}$, harvested
629 at indicated time points and probed with indicated antibodies and by heme peroxidase
630 activity detection using enhanced chemiluminescence (ECL). β -CF₁ is an internal loading
631 control. Samples were loaded at least three times on mirror gels.

632 **Figure S2: respiratory metabolism and chlororespiration**

633 **(A)** Peroxidase activity of heme c groups from total extracts of WT-S24 starved in
634 heterotrophy. The peroxidase activity was assessed as in Vargas et al., 1993 at indicated
635 time points in absence or presence of NO donors (either SNP or SNAP) or of the NO
636 scavenger cPTIO.

637 **(B)** Chlororespiratory activity of Δ petA cells in TAP and in TAP-S after 48 hours of
638 starvation.

639 Measurements were taken as in (Houille-Vernes et al., 2011). Results show the mean of
640 3 independent experiments \pm SEM. Data were normalized to F_M taken in TAP conditions.

641 **Figure S3. Effects of sulfur deprivation in darkness and in heterotrophy on WT-S24⁻
642 and WT T222⁺.**

643 **(A)** Evolution of Φ_{PSII} and F_V/F_M during sulfur starvation of strain WT-S24⁻ (diamonds), and
644 WT T222⁺ (stars) in TAP-S and complete darkness. Data represent the mean of 3
645 independent experiments \pm SEM.

646 **(B)** Evolution of Φ_{PSII} and F_V/F_M of one representative tetrad obtained from crossing of
647 WT-S24⁻ and WT T222⁺.

648 **Figure S4. Sulfur starvation on the *ftsh1-1* and *clpP_{AUU}* mutants, defective for
649 protease function.**

650 **(A)** Comparison of photosynthetic parameters evolution, Φ_{PSII} (top) and F_V/F_M (bottom),
651 for WT-S24 and *ftsh1-1* under starvation in TAP-S and $15 \mu E \cdot m^{-2} \cdot s^{-1}$.

652 **(B)** Comparison of photosynthetic parameters evolution, Φ_{PSII} (top) and F_V/F_M (bottom),
653 for WT-S24⁻ and *clpP_{AUU}* under starvation in TAP-S and $15 \mu E \cdot m^{-2} \cdot s^{-1}$.

654 **(C)** Residual photosynthetic efficiency (as % of the initial efficiency) after 72h of starvation
655 between WT-S24⁻, *ftsh1-1* and *clpP_{AUU}*.

656 Data represent the mean of 5 independent experiments \pm SEM.

657 **Figure S5. DAF-FM DA fluorescence can be seen only in presence of nitric oxide or
658 under sulfur starvation.**

659 Visualization of NO production *in vivo*, using the DAF-FM DA (5 μ M) probe. Cells were
660 harvested and observed with a fluorescence microscope after washing step and 10-fold
661 concentration. CHLORO, chlorophyll autofluorescence; DAF-FM DA, NO-dependent
662 green fluorescence; MERGE, chlorophyll and NO-dependent signals visualized together.
663 From left to right panels: Cells in replete medium; cells in replete medium incubated with
664 DEA NONOate (0.1 mM); starved cells after 48 hours; starved cells after 48 hours
665 incubated 1 hour with NO-scavenger cPTIO (0.2 mM).

666 **Figure S6. Effects on photosynthetic parameters of cPTIO alone or in the presence**
667 **of NO donors.**

668 **(A)** Φ_{PSII} and F_V/F_M evolution measured after addition of cPTIO (0.1 mM) every 24 hours.
669 Data show the mean of three independent experiments \pm SEM.

670 **(B)** Effects on photosynthetic efficiency of SNAP (0.05 mM) and cPTIO (0.2 mM), added
671 alone or together.

672 **(C)** Effects on photosynthetic efficiency of SNP (0.5 mM) and cPTIO (0.2 mM), added
673 alone or together.

674 Black arrows indicate drug addition, experiments were performed in TAP-S at $15 \mu\text{E}\cdot\text{m}^{-2}\cdot\text{s}^{-1}$.
675

676 **Figure S7. Effects of NO-donors/scavenger and NO-synthesis inhibitors on**
677 **photosynthetic parameters in sulfur replete conditions.**

678 **(A)** Effects of NO-scavenger/donors on Φ_{PSII} (top) and F_V/F_M (bottom) of WT-S24⁻ cells
679 kept in TAP at $15 \mu\text{E}\cdot\text{m}^{-2}\cdot\text{s}^{-1}$.

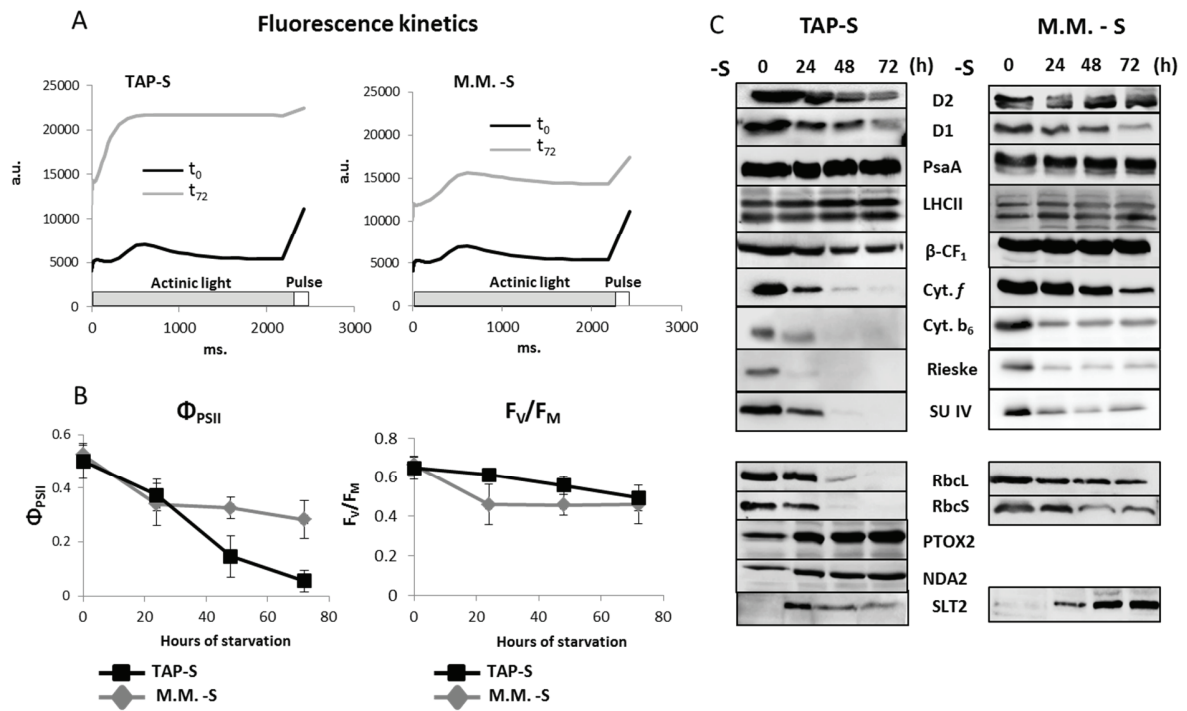
680 **(B)** Effects of NO synthesis inhibitors (1 mM final concentration for all) on Φ_{PSII} (top) and
681 F_V/F_M (bottom) of WT-S24⁻ cells kept in TAP at $15 \mu\text{E}\cdot\text{m}^{-2}\cdot\text{s}^{-1}$.

682 Arrows indicate drugs addition.

683 **Figure S8: Total glutathione content of cell extracts during sulfur starvation**

684 Samples were harvested at indicated times during sulfur starvation in TAP-S and analyzed
685 as in (Queval and Noctor, 2007) and (Perez-Martin et al., 2014). Data represent the mean
686 of 3 independent experiments \pm SEM.

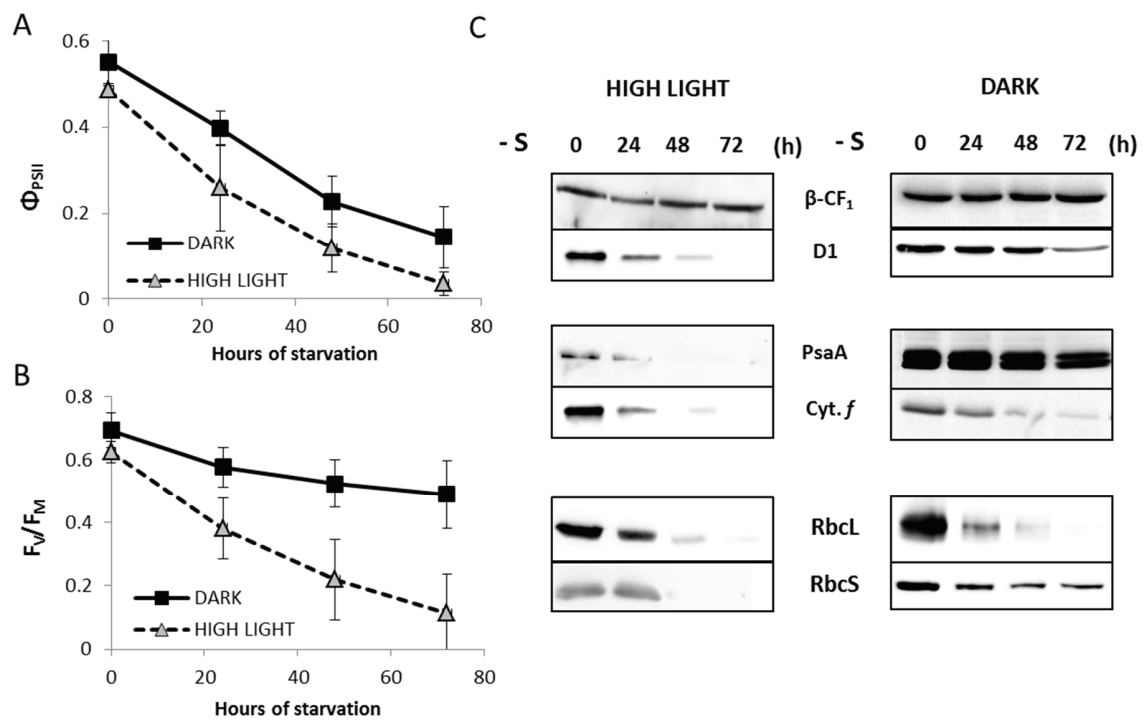
687
688 Supplemental dataset 1: This compressed folder contains all raw images of western blots
689 used to prepare composite figures.



690

691 Figure 1

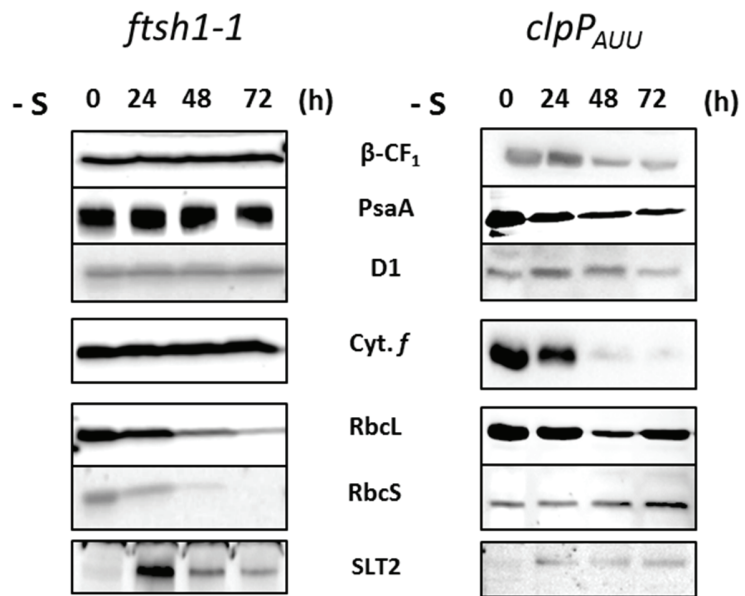
692



693

694 Figure 2

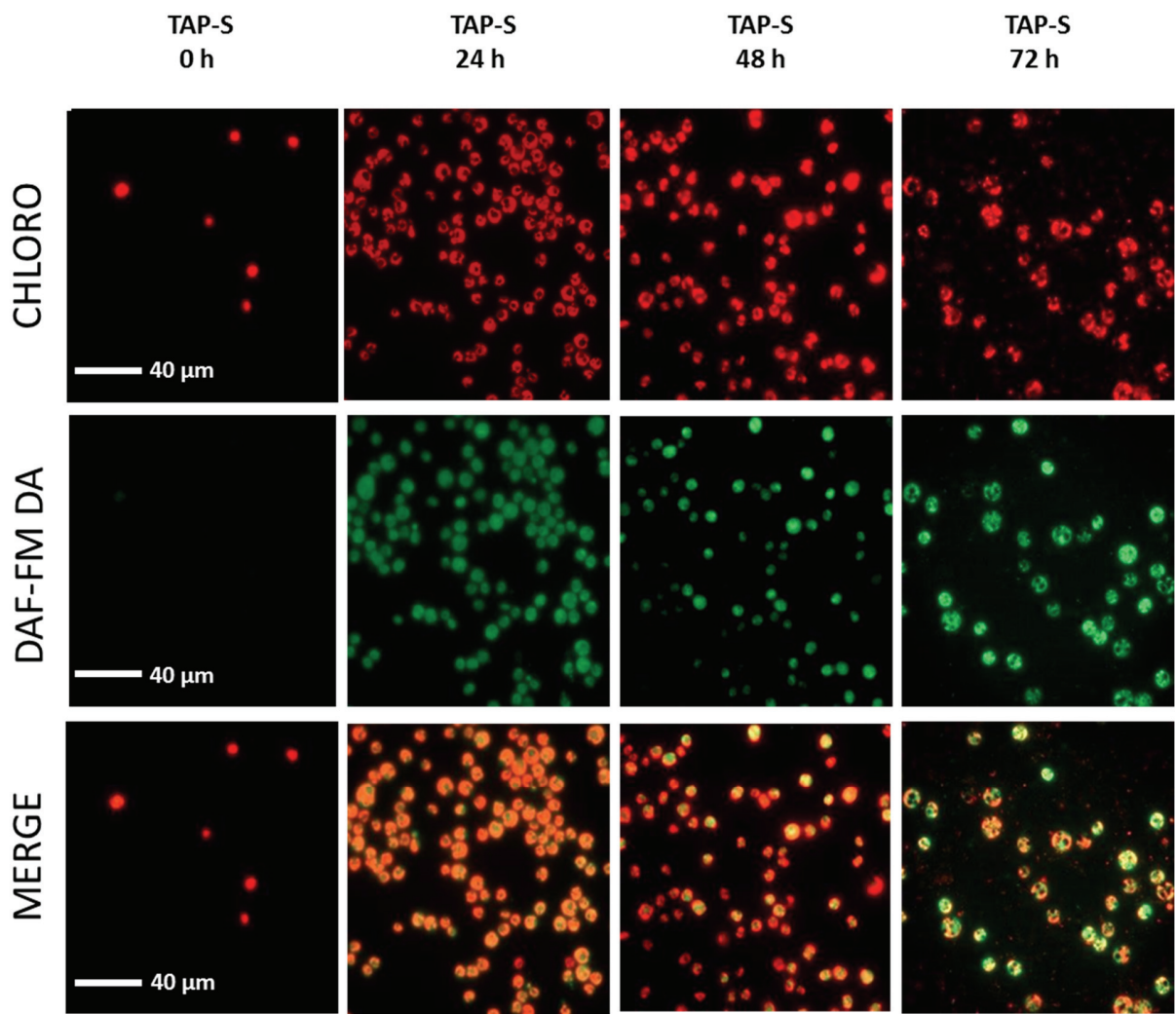
695



696

697 Figure 3

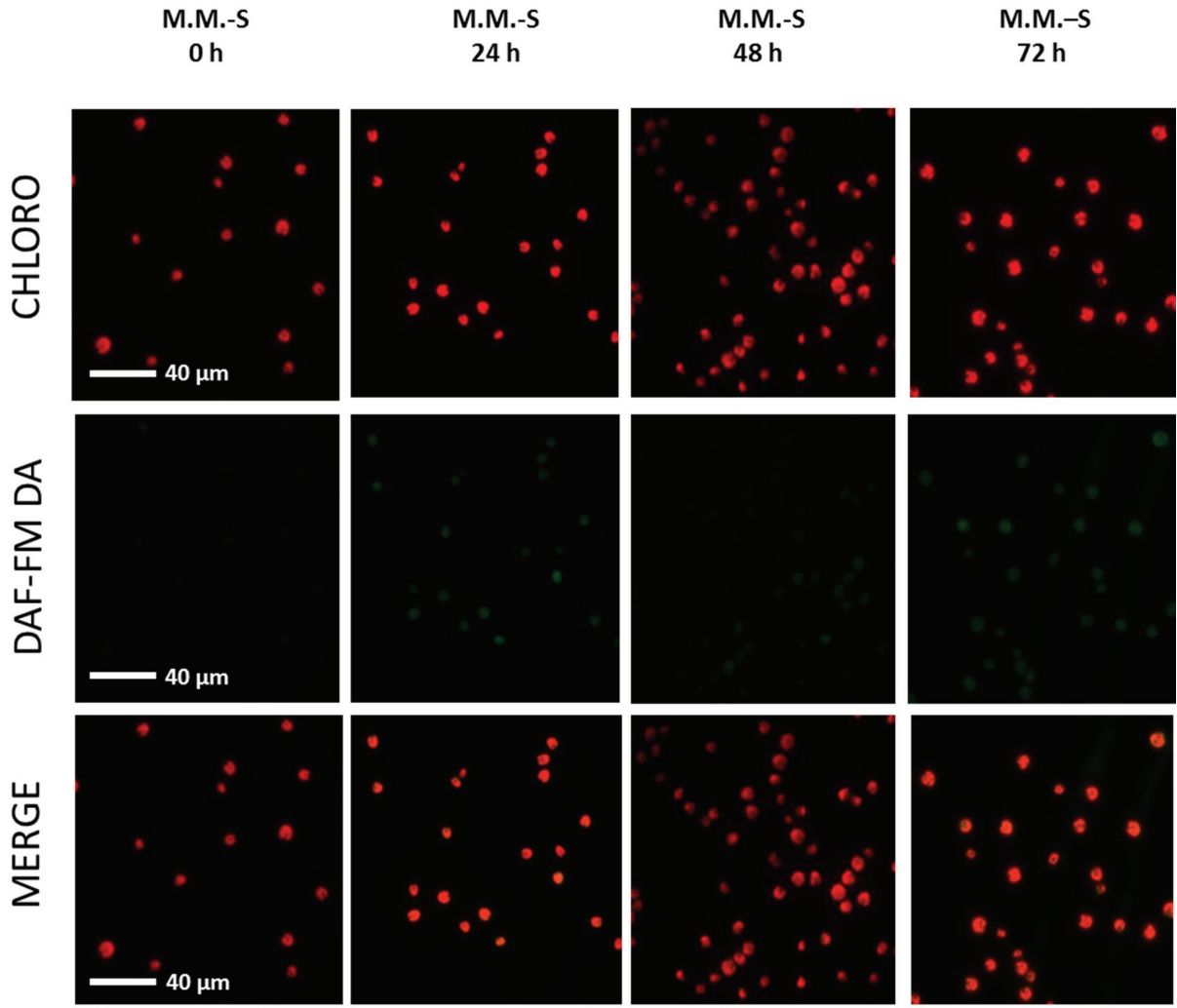
698



699

700 Figure 4

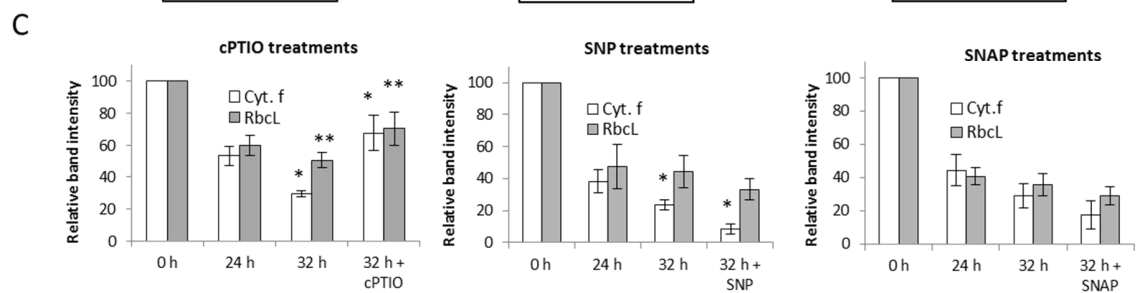
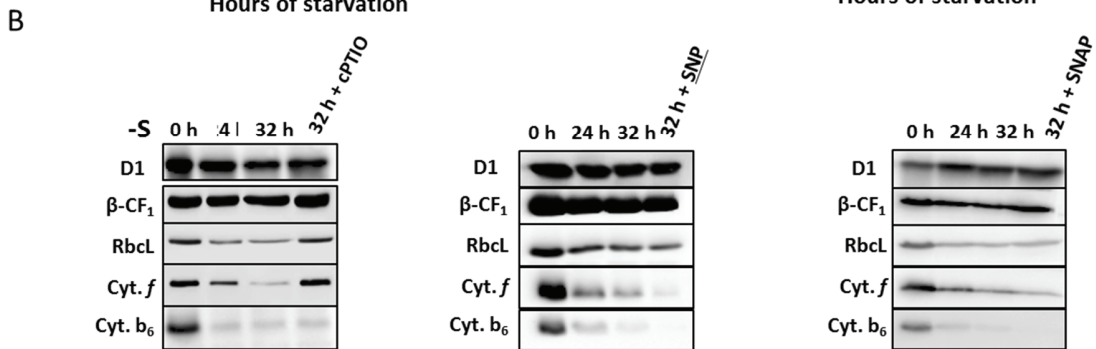
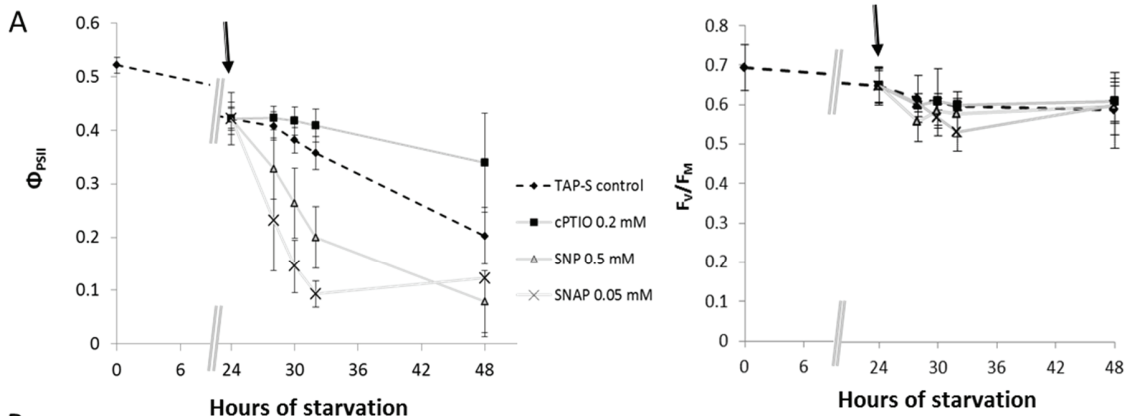
701



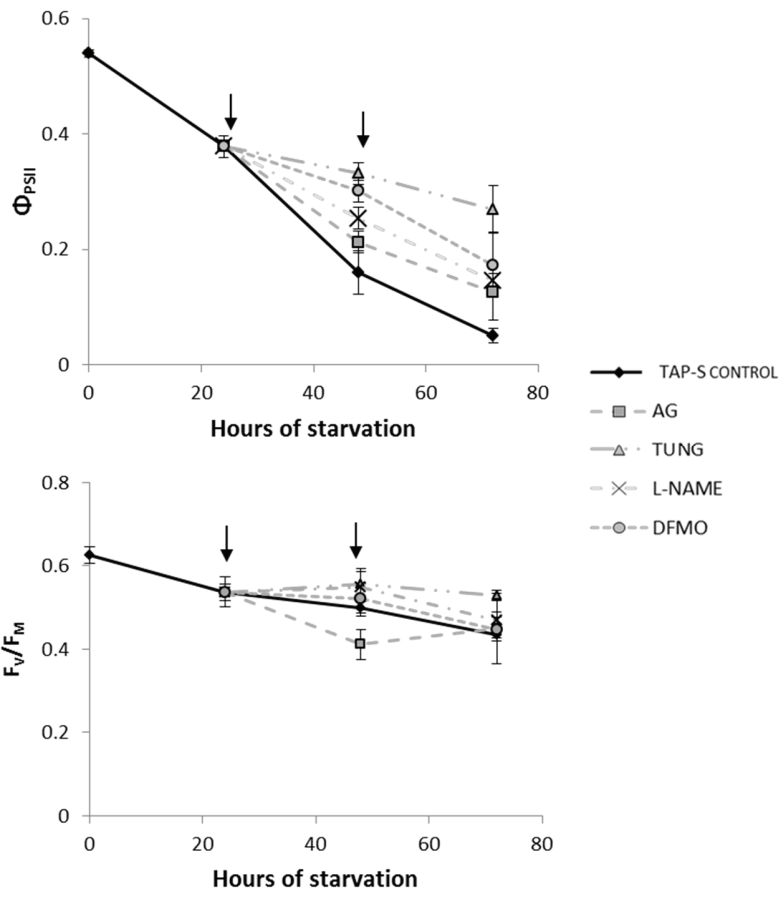
702

703 Figure 5

704



705
706 Figure 6
707



708

709 Figure 7

710

734 **Bibliography**

- 735 **Antal TK, Krendeleva TE, Laurinavichene TV, Makarova VV, Ghirardi ML, Rubin AB, Tsygankov AA,**
736 **Seibert M** (2003) The dependence of algal H₂ production on Photosystem II and O₂ consumption
737 activities in sulfur-deprived *Chlamydomonas reinhardtii* cells. *Biochim Biophys Acta* **1607**: 153-
738 160
- 739 **Astier J, Lindermayr C** (2012) Nitric oxide-dependent posttranslational modification in plants: an update.
740 *Int J Mol Sci* **13**: 15193-15208
- 741 **Baek K, Kim DH, Jeong J, Sim SJ, Melis A, Kim JS, Jin E, Bae S** (2016) DNA-free two-gene knockout in
742 *Chlamydomonas reinhardtii* via CRISPR-Cas9 ribonucleoproteins. *Sci Rep* **6**: 30620
- 743 **Baek K, Yu J, Jeong J, Sim SJ, Bae S, Jin E** (2018) Photoautotrophic production of macular pigment in a
744 *Chlamydomonas reinhardtii* strain generated by using DNA-free CRISPR-Cas9 RNP-mediated
745 mutagenesis. *Biotechnol Bioeng* **115**: 719-728
- 746 **Barroso JB, Corpas FJ, Carreras A, Sandalio LM, Valderrama R, Palma JM, Lupianez JA, del Rio LA** (1999)
747 Localization of nitric-oxide synthase in plant peroxisomes. *J Biol Chem* **274**: 36729-36733
- 748 **Baudouin E, Pieuchot L, Engler G, Pauly N, Puppo A** (2006) Nitric oxide is formed in *Medicago*
749 *truncatula*-*Sinorhizobium meliloti* functional nodules. *Mol Plant Microbe Interact* **19**: 970-975
- 750 **Beligni MV, Lamattina L** (2000) Nitric oxide stimulates seed germination and de-etiolation, and inhibits
751 hypocotyl elongation, three light-inducible responses in plants. *Planta* **210**: 215-221
- 752 **Besson-Bard A, Gravot A, Richaud P, Auroy P, Duc C, Gaymard F, Taconnat L, Renou JP, Pugin A,**
753 **Wendehenne D** (2009) Nitric oxide contributes to cadmium toxicity in *Arabidopsis* by promoting
754 cadmium accumulation in roots and by up-regulating genes related to iron uptake. *Plant Physiol*
755 **149**: 1302-1315
- 756 **Blaby-Haas CE, Merchant SS** (2017) Regulating cellular trace metal economy in algae. *Curr Opin Plant*
757 *Biol* **39**: 88-96
- 758 **Bulte L, Bennoun P** (1990) Translational accuracy and sexual differentiation in *Chlamydomonas*
759 *reinhardtii*. *Curr.Genet.* **18**: 155-160
- 760 **Bulte L, Wollman FA** (1990) Mechanism and control of the inactivation of cytochrome *b6/f* complexes during
761 gametogenesis in *C. reinhardtii*. In M Baltscheffsky, ed, *Current Research in Photosynthesis*, Vol
762 3, pp 715-718
- 763 **Bulte L, Wollman FA** (1992) Evidence for a selective destabilization of an integral membrane protein, the
764 cytochrome *b6/f* complex, during gametogenesis in *Chlamydomonas reinhardtii*. *Eur J Biochem*
765 **204**: 327-336
- 766 **Chamizo-Ampudia A, Sanz-Luque E, Llamas A, Ocana-Calahorra F, Mariscal V, Carreras A, Barroso JB,**
767 **Galvan A, Fernandez E** (2016) A dual system formed by the ARC and NR molybdoenzymes
768 mediates nitrite-dependent NO production in *Chlamydomonas*. *Plant Cell Environ* **39**: 2097-2107
- 769 **Chaux F, Burlacot A, Mekhalfi M, Auroy P, Blangy S, Richaud P, Peltier G** (2017) Flavodiiron Proteins
770 Promote Fast and Transient O₂ Photoreduction in *Chlamydomonas*. *Plant Physiol* **174**: 1825-
771 1836
- 772 **Corpas FJ, Barroso JB, Carreras A, Quiros M, Leon AM, Romero-Puertas MC, Esteban FJ, Valderrama R,**
773 **Palma JM, Sandalio LM, Gomez M, del Rio LA** (2004) Cellular and subcellular localization of
774 endogenous nitric oxide in young and senescent pea plants. *Plant Physiol* **136**: 2722-2733
- 775 **Delledonne M, Xia Y, Dixon RA, Lamb C** (1998) Nitric oxide functions as a signal in plant disease
776 resistance. *Nature* **394**: 585-588
- 777 **Desplats C, Mus F, Cuine S, Billon E, Cournac L, Peltier G** (2009) Characterization of Nda2, a
778 plastoquinone-reducing type II NAD(P)H dehydrogenase in *chlamydomonas* chloroplasts. *J Biol*
779 *Chem* **284**: 4148-4157

780 **Dong Y, Silbermann M, Speiser A, Forieri I, Linster E, Poschet G, Allboje Samami A, Wanatabe M, Sticht**
781 **C, Teleman AA, Deragon JM, Saito K, Hell R, Wirtz M** (2017) Sulfur availability regulates plant
782 growth via glucose-TOR signaling. *Nat Commun* **8**: 1174
783 **Drapier D, Girard-Bascou J, Wollman FA** (1992) Evidence for Nuclear Control of the Expression of the
784 *atpA* and *atpB* Chloroplast Genes in *Chlamydomonas*. *Plant Cell* **4**: 283-295
785 **Fang SC, Chung CL, Chen CH, Lopez-Paz C, Umen JG** (2014) Defects in a new class of sulfate/anion
786 transporter link sulfur acclimation responses to intracellular glutathione levels and cell cycle
787 control. *Plant Physiol* **166**: 1852-1868
788 **Feechan A, Kwon E, Yun BW, Wang Y, Pallas JA, Loake GJ** (2005) A central role for S-nitrosothiols in
789 plant disease resistance. *Proc Natl Acad Sci U S A* **102**: 8054-8059
790 **Ferenczi A, Pyott DE, Xipnitou A, Molnar A** (2017) Efficient targeted DNA editing and replacement in
791 *Chlamydomonas reinhardtii* using Cpf1 ribonucleoproteins and single-stranded DNA. *Proc Natl*
792 *Acad Sci U S A* **114**: 13567-13572
793 **Forestier M, King P, Zhang L, Posewitz M, Schwarzer S, Happe T, Ghirardi ML, Seibert M** (2003)
794 Expression of two [Fe]-hydrogenases in *Chlamydomonas reinhardtii* under anaerobic conditions.
795 *Eur J Biochem* **270**: 2750-2758
796 **Gallaher SD, Fitz-Gibbon ST, Glaesener AG, Pellegrini M, Merchant SS** (2015) *Chlamydomonas* Genome
797 Resource for Laboratory Strains Reveals a Mosaic of Sequence Variation, Identifies True Strain
798 Histories, and Enables Strain-Specific Studies. *Plant Cell* **27**: 2335-2352
799 **Garcia-Mata C, Lamattina L** (2001) Nitric oxide induces stomatal closure and enhances the adaptive
800 plant responses against drought stress. *Plant Physiol* **126**: 1196-1204
801 **Georgakopoulos JH, Sokolenko A, Arkas M, Sofou G, Herrmann RG, Argyroudi-Akoyunoglou JH** (2002)
802 Proteolytic activity against the light-harvesting complex and the D1/D2 core proteins of
803 Photosystem II in close association to the light-harvesting complex II trimer. *Biochim Biophys*
804 *Acta* **1556**: 53-64
805 **Gerotto C, Alboresi A, Meneghesso A, Jokel M, Suorsa M, Aro EM, Morosinotto T** (2016) Flavodiiron
806 proteins act as safety valve for electrons in *Physcomitrella patens*. *Proc Natl Acad Sci U S A* **113**:
807 12322-12327
808 **Ghirardi ML, Zhang L, Lee JW, Flynn T, Seibert M, Greenbaum E, Melis A** (2000) Microalgae: a green
809 source of renewable H₂. *Trends Biotechnol* **18**: 506-511
810 **Gibbs DJ, Md Isa N, Movahedi M, Lozano-Juste J, Mendiondo GM, Berckhan S, Marin-de la Rosa N,**
811 **Vicente Conde J, Sousa Correia C, Pearce SP, Bassel GW, Hamali B, Talloji P, Tome DF, Coego A,**
812 **Beynon J, Alabadi D, Bachmair A, Leon J, Gray JE, Theodoulou FL, Holdsworth MJ** (2014) Nitric
813 oxide sensing in plants is mediated by proteolytic control of group VII ERF transcription factors.
814 *Mol Cell* **53**: 369-379
815 **Giordano M, Pezzoni V, Hell R** (2000) Strategies for the allocation of resources under sulfur limitation in
816 the green alga *Dunaliella salina*. *Plant Physiol* **124**: 857-864
817 **Gonzalez-Ballester D, Casero D, Cokus S, Pellegrini M, Merchant SS, Grossman AR** (2010) RNA-seq
818 analysis of sulfur-deprived *Chlamydomonas* cells reveals aspects of acclimation critical for cell
819 survival. *Plant Cell* **22**: 2058-2084
820 **Graziano M, Beligni MV, Lamattina L** (2002) Nitric oxide improves internal iron availability in plants.
821 *Plant Physiol* **130**: 1852-1859
822 **Greiner A, Kelterborn S, Evers H, Kreimer G, Sizova I, Hegemann P** (2017) Targeting of Photoreceptor
823 Genes in *Chlamydomonas reinhardtii* via Zinc-Finger Nucleases and CRISPR/Cas9. *Plant Cell* **29**:
824 2498-2518
825 **Grossman A** (2000) Acclimation of *Chlamydomonas reinhardtii* to its nutrient environment. *Protist* **151**:
826 201-224

- 827 **Grossman AR, Catalanotti C, Yang W, Dubini A, Magneschi L, Subramanian V, Posewitz MC, Seibert M**
828 (2011) Multiple facets of anoxic metabolism and hydrogen production in the unicellular green
829 alga *Chlamydomonas reinhardtii*. *New Phytol* **190**: 279-288
- 830 **Grossman AR, Croft M, Gladyshev VN, Merchant SS, Posewitz MC, Prochnik S, Spalding MH** (2007)
831 Novel metabolism in *Chlamydomonas* through the lens of genomics. *Curr Opin Plant Biol* **10**:
832 190-198
- 833 **Harris EH** (1989) *The Chlamydomonas source book: a comprehensive guide to biology and laboratory*
834 *use*. Academic Press, San Diego
- 835 **He Y, Tang RH, Hao Y, Stevens RD, Cook CW, Ahn SM, Jing L, Yang Z, Chen L, Guo F, Fiorani F, Jackson**
836 **RB, Crawford NM, Pei ZM** (2004) Nitric oxide represses the *Arabidopsis* floral transition. *Science*
837 **305**: 1968-1971
- 838 **Hemschemeier A, Duner M, Casero D, Merchant SS, Winkler M, Happe T** (2013) Hypoxic survival
839 requires a 2-on-2 hemoglobin in a process involving nitric oxide. *Proc Natl Acad Sci U S A* **110**:
840 10854-10859
- 841 **Hemschemeier A, Fouchard S, Cournac L, Peltier G, Happe T** (2008) Hydrogen production by
842 *Chlamydomonas reinhardtii*: an elaborate interplay of electron sources and sinks. *Planta* **227**:
843 397-407
- 844 **Houille-Vernes L, Rappaport F, Wollman FA, Alric J, Johnson X** (2011) Plastid terminal oxidase 2 (PTOX2)
845 is the major oxidase involved in chlororespiration in *Chlamydomonas*. *Proc Natl Acad Sci U S A*
846 **108**: 20820-20825
- 847 **Irihimovitch V, Stern DB** (2006) The sulfur acclimation SAC3 kinase is required for chloroplast
848 transcriptional repression under sulfur limitation in *Chlamydomonas reinhardtii*. *Proc Natl Acad*
849 *Sci U S A* **103**: 7911-7916
- 850 **Jacques S, Ghesquiere B, Van Breusegem F, Gevaert K** (2013) Plant proteins under oxidative attack.
851 *Proteomics* **13**: 932-940
- 852 **Jokel M, Kosourov S, Battchikova N, Tsygankov AA, Aro EM, Allahverdiyeva Y** (2015) *Chlamydomonas*
853 *Flavodiiron Proteins Facilitate Acclimation to Anoxia During Sulfur Deprivation*. *Plant Cell Physiol*
854 **56**: 1598-1607
- 855 **Kajikawa M, Sawaragi Y, Shinkawa H, Yamano T, Ando A, Kato M, Hirono M, Sato N, Fukuzawa H**
856 (2015) Algal dual-specificity tyrosine phosphorylation-regulated kinase, triacylglycerol
857 accumulation regulator1, regulates accumulation of triacylglycerol in nitrogen or sulfur
858 deficiency. *Plant Physiol* **168**: 752-764
- 859 **Kopriva S, Rennenberg H** (2004) Control of sulphate assimilation and glutathione synthesis: interaction
860 with N and C metabolism. *J Exp Bot* **55**: 1831-1842
- 861 **Kornberg MD, Sen N, Hara MR, Juluri KR, Nguyen JV, Snowman AM, Law L, Hester LD, Snyder SH** (2010)
862 GAPDH mediates nitrosylation of nuclear proteins. *Nat Cell Biol* **12**: 1094-1100
- 863 **Kosourov S, Seibert M, Ghirardi ML** (2003) Effects of extracellular pH on the metabolic pathways in
864 sulfur-deprived, H₂-producing *Chlamydomonas reinhardtii* cultures. *Plant Cell Physiol* **44**: 146-
865 155
- 866 **Kuras R, Wollman FA** (1994) The assembly of cytochrome b6/f complexes: an approach using genetic
867 transformation of the green alga *Chlamydomonas reinhardtii*. *EMBO J* **13**: 1019-1027
- 868 **Lee CM, Kim BY, Li L, Morgan ET** (2008) Nitric oxide-dependent proteasomal degradation of cytochrome
869 P450 2B proteins. *J Biol Chem* **283**: 889-898
- 870 **Lee U, Wie C, Fernandez BO, Feelisch M, Vierling E** (2008) Modulation of nitrosative stress by S-
871 nitroglutathione reductase is critical for thermotolerance and plant growth in *Arabidopsis*.
872 *Plant Cell* **20**: 786-802
- 873 **Leustek T, Saito K** (1999) Sulfate transport and assimilation in plants. *Plant Physiol* **120**: 637-644

874 **Lindermayr C, Sell S, Muller B, Leister D, Durner J** (2010) Redox regulation of the NPR1-TGA1 system of
875 *Arabidopsis thaliana* by nitric oxide. *Plant Cell* **22**: 2894-2907

876 **Maia LB, Moura JJ** (2011) Nitrite reduction by xanthine oxidase family enzymes: a new class of nitrite
877 reductases. *J Biol Inorg Chem* **16**: 443-460

878 **Majeran W, Wollman FA, Vallon O** (2000) Evidence for a role of ClpP in the degradation of the
879 chloroplast cytochrome b(6)f complex. *Plant Cell* **12**: 137-150

880 **Malnoe A, Wang F, Girard-Bascou J, Wollman FA, de Vitry C** (2014) Thylakoid FtsH protease contributes
881 to photosystem II and cytochrome b6f remodeling in *Chlamydomonas reinhardtii* under stress
882 conditions. *Plant Cell* **26**: 373-390

883 **Mata-Perez C, Begara-Morales JC, Chaki M, Sanchez-Calvo B, Valderrama R, Padilla MN, Corpas FJ,**
884 **Barroso JB** (2016) Protein Tyrosine Nitration during Development and Abiotic Stress Response in
885 Plants. *Front Plant Sci* **7**: 1699

886 **Melis A, Zhang L, Forestier M, Ghirardi ML, Seibert M** (2000) Sustained photobiological hydrogen gas
887 production upon reversible inactivation of oxygen evolution in the green alga *Chlamydomonas*
888 *reinhardtii*. *Plant Physiol* **122**: 127-136

889 **Merchant SS, Helmann JD** (2012) Elemental economy: microbial strategies for optimizing growth in the
890 face of nutrient limitation. *Adv Microb Physiol* **60**: 91-210

891 **Michelet L, Zaffagnini M, Morisse S, Sparla F, Pérez-Pérez ME, Francia F, Danon A, Marchand CH,**
892 **Fermani S, Trost P, Lemaire SD** (2013) Redox regulation of the Calvin-Benson cycle: something
893 old, something new. *Front Plant Sci* **4**: 470

894 **Minaeva E, Zalutskaya Z, Filina V, Ermilova E** (2017) Truncated hemoglobin 1 is a new player in
895 *Chlamydomonas reinhardtii* acclimation to sulfur deprivation. *PLoS One* **12**: e0186851

896 **Mishina TE, Lamb C, Zeier J** (2007) Expression of a nitric oxide degrading enzyme induces a senescence
897 programme in *Arabidopsis*. *Plant Cell Environ* **30**: 39-52

898 **Morisse S, Zaffagnini M, Gao XH, Lemaire SD, Marchand CH** (2014) Insight into protein S-nitrosylation in
899 *Chlamydomonas reinhardtii*. *Antioxid Redox Signal* **21**: 1271-1284

900 **Nagy V, Vidal-Meireles A, Podmaniczki A, Szentmihalyi K, Rakhely G, Zsigmond L, Kovacs L, Toth SZ**
901 (2018) The mechanism of photosystem-II inactivation during sulphur deprivation-induced H₂
902 production in *Chlamydomonas reinhardtii*. *Plant J* **94**: 548-561

903 **Nagy V, Vidal-Meireles A, Tengolics R, Rakhely G, Garab G, Kovacs L, Toth SZ** (2016) Ascorbate
904 accumulation during sulphur deprivation and its effects on photosystem II activity and H₂
905 production of the green alga *Chlamydomonas reinhardtii*. *Plant Cell Environ* **39**: 1460-1472

906 **Nakamura T, Lipton SA** (2013) Emerging role of protein-protein transnitrosylation in cell signaling
907 pathways. *Antioxid Redox Signal* **18**: 239-249

908 **Neill SJ, Desikan R, Clarke A, Hurst RD, Hancock JT** (2002) Hydrogen peroxide and nitric oxide as
909 signalling molecules in plants. *J Exp Bot* **53**: 1237-1247

910 **Obata T, Fernie AR** (2012) The use of metabolomics to dissect plant responses to abiotic stresses. *Cell*
911 *Mol Life Sci* **69**: 3225-3243

912 **Ouellet H, Ouellet Y, Richard C, Labarre M, Wittenberg B, Wittenberg J, Guertin M** (2002) Truncated
913 hemoglobin HbN protects *Mycobacterium bovis* from nitric oxide. *Proc Natl Acad Sci U S A* **99**:
914 5902-5907

915 **Pagnussat GC, Simontacchi M, Puntarulo S, Lamattina L** (2002) Nitric oxide is required for root
916 organogenesis. *Plant Physiol* **129**: 954-956

917 **Perazzolli M, Dominici P, Romero-Puertas MC, Zago E, Zeier J, Sonoda M, Lamb C, Delledonne M** (2004)
918 *Arabidopsis* nonsymbiotic hemoglobin AHB1 modulates nitric oxide bioactivity. *Plant Cell* **16**:
919 2785-2794

920 **Perazzolli M, Romero-Puertas MC, Delledonne M** (2006) Modulation of nitric oxide bioactivity by plant
921 haemoglobins. *J Exp Bot* **57**: 479-488

922 **Perez-Martin M, Perez-Perez ME, Lemaire SD, Crespo JL** (2014) Oxidative stress contributes to
923 autophagy induction in response to endoplasmic reticulum stress in *Chlamydomonas reinhardtii*.
924 *Plant Physiol* **166**: 997-1008

925 **Picard-Bennoun M, Bennoun P** (1985) Change in cytoplasmic ribosome properties during gametogenesis
926 in the alga *Chlamydomonas reinhardtii*. *Curr Genet* **9**: 239-243

927 **Pollock SV, Pootakham W, Shibagaki N, Moseley JL, Grossman AR** (2005) Insights into the acclimation of
928 *Chlamydomonas reinhardtii* to sulfur deprivation. *Photosynth Res* **86**: 475-489

929 **Prado AM, Porterfield DM, Feijo JA** (2004) Nitric oxide is involved in growth regulation and re-
930 orientation of pollen tubes. *Development* **131**: 2707-2714

931 **Queval G, Noctor G** (2007) A plate reader method for the measurement of NAD, NADP, glutathione, and
932 ascorbate in tissue extracts: Application to redox profiling during *Arabidopsis* rosette
933 development. *Anal Biochem* **363**: 58-69

934 **Quisel JD, Wykoff DD, Grossman AR** (1996) Biochemical characterization of the extracellular
935 phosphatases produced by phosphorus-deprived *Chlamydomonas reinhardtii*. *Plant Physiol* **111**:
936 839-848

937 **Sakihama Y, Nakamura S, Yamasaki H** (2002) Nitric oxide production mediated by nitrate reductase in
938 the green alga *Chlamydomonas reinhardtii*: an alternative NO production pathway in
939 photosynthetic organisms. *Plant Cell Physiol* **43**: 290-297

940 **Saroussi S, Sanz-Luque E, Kim RG, Grossman AR** (2017) Nutrient scavenging and energy management:
941 acclimation responses in nitrogen and sulfur deprived *Chlamydomonas*. *Curr Opin Plant Biol* **39**:
942 114-122

943 **Schmollinger S, Schulz-Raffelt M, Strenkert D, Veyel D, Vallon O, Schroda M** (2013) Dissecting the heat
944 stress response in *Chlamydomonas* by pharmaceutical and RNAi approaches reveals conserved
945 and novel aspects. *Mol Plant* **6**: 1795-1813

946 **Schreiner Ø, Lien T, Knutsen G** (1975) The capacity for arylsulfatase synthesis in synchronous and
947 synchronized cultures of *Chlamydomonas reinhardtii*. *Biochimica et Biophysica Acta (BBA) -*
948 *Enzymology* **384**: 180-193

949 **Sears BB, Boynton JE, Gillham NW** (1980) The Effect of Gametogenesis Regimes on the Chloroplast
950 Genetic System of *CHLAMYDOMONAS REINHARDTII*. *Genetics* **96**: 95-114

951 **Shin SE, Lim JM, Koh HG, Kim EK, Kang NK, Jeon S, Kwon S, Shin WS, Lee B, Hwangbo K, Kim J, Ye SH,**
952 **Yun JY, Seo H, Oh HM, Kim KJ, Kim JS, Jeong WJ, Chang YK, Jeong BR** (2016) CRISPR/Cas9-
953 induced knockout and knock-in mutations in *Chlamydomonas reinhardtii*. *Sci Rep* **6**: 27810

954 **Sizova I, Greiner A, Awasthi M, Kateriya S, Hegemann P** (2013) Nuclear gene targeting in
955 *Chlamydomonas* using engineered zinc-finger nucleases. *Plant J* **73**: 873-882

956 **Smagghe BJ, Trent JT, 3rd, Hargrove MS** (2008) NO dioxygenase activity in hemoglobins is ubiquitous in
957 vitro, but limited by reduction in vivo. *PLoS ONE* **3**: e2039

958 **Sokolenko A, Pojidaeva E, Zinchenko V, Panichkin V, Glaser VM, Herrmann RG, Shestakov SV** (2002)
959 The gene complement for proteolysis in the cyanobacterium *Synechocystis* sp. PCC 6803 and
960 *Arabidopsis thaliana* chloroplasts. *Curr Genet* **41**: 291-310

961 **Stamler JS, Hess DT** (2010) Nascent nitrosylases. *Nat Cell Biol* **12**: 1024-1026

962 **Stroebel D, Choquet Y, Popot JL, Picot D** (2003) An atypical haem in the cytochrome b(6)f complex.
963 *Nature* **426**: 413-418

964 **Sugimoto K, Sato N, Tsuzuki M** (2007) Utilization of a chloroplast membrane sulfolipid as a major
965 internal sulfur source for protein synthesis in the early phase of sulfur starvation in
966 *Chlamydomonas reinhardtii*. *FEBS Lett* **581**: 4519-4522

967 **Tada Y, Spoel SH, Pajerowska-Mukhtar K, Mou Z, Song J, Wang C, Zuo J, Dong X** (2008) Plant immunity
968 requires conformational changes [corrected] of NPR1 via S-nitrosylation and thioredoxins.
969 *Science* **321**: 952-956

970 **Tewari RK, Kumar P, Kim S, Hahn EJ, Paek KY** (2009) Nitric oxide retards xanthine oxidase-mediated
971 superoxide anion generation in Phalaenopsis flower: an implication of NO in the senescence and
972 oxidative stress regulation. *Plant Cell Rep* **28**: 267-279

973 **Tun NN, Santa-Catarina C, Begum T, Silveira V, Handro W, Floh EI, Scherer GF** (2006) Polyamines induce
974 rapid biosynthesis of nitric oxide (NO) in Arabidopsis thaliana seedlings. *Plant Cell Physiol* **47**:
975 346-354

976 **Vallon O, Bulte L, Kuras R, Olive J, Wollman FA** (1993) Extensive accumulation of an extracellular L-
977 amino-acid oxidase during gametogenesis of Chlamydomonas reinhardtii. *Eur J Biochem* **215**:
978 351-360

979 **Vargas C, McEwan AG, Downie JA** (1993) Detection of c-type cytochromes using enhanced
980 chemiluminescence. *Anal Biochem* **209**: 323-326

981 **Wang BL, Tang XY, Cheng LY, Zhang AZ, Zhang WH, Zhang FS, Liu JQ, Cao Y, Allan DL, Vance CP, Shen JB**
982 (2010) Nitric oxide is involved in phosphorus deficiency-induced cluster-root development and
983 citrate exudation in white lupin. *New Phytol* **187**: 1112-1123

984 **Wei L, Derrien B, Gautier A, Houille-Vernes L, Boulouis A, Saint-Marcoux D, Malnoe A, Rappaport F, de**
985 **Vitry C, Vallon O, Choquet Y, Wollman FA** (2014) Nitric oxide-triggered remodeling of
986 chloroplast bioenergetics and thylakoid proteins upon nitrogen starvation in Chlamydomonas
987 reinhardtii. *Plant Cell* **26**: 353-372

988 **Wendehenne D, Hancock JT** (2011) New frontiers in nitric oxide biology in plant. *Plant Sci* **181**: 507-508

989 **Wykoff DD, Davies JP, Melis A, Grossman AR** (1998) The regulation of photosynthetic electron transport
990 during nutrient deprivation in Chlamydomonas reinhardtii. *Plant Physiol* **117**: 129-139

991 **Yamasaki H, Cohen MF** (2006) NO signal at the crossroads: polyamine-induced nitric oxide synthesis in
992 plants? *Trends Plant Sci* **11**: 522-524

993 **Yang D, Song D, Kind T, Ma Y, Hoefkens J, Fiehn O** (2015) Lipidomic Analysis of Chlamydomonas
994 reinhardtii under Nitrogen and Sulfur Deprivation. *PLoS ONE* **10**: e0137948

995 **Yehudai-Resheff S, Zimmer SL, Komine Y, Stern DB** (2007) Integration of chloroplast nucleic acid
996 metabolism into the phosphate deprivation response in Chlamydomonas reinhardtii. *Plant Cell*
997 **19**: 1023-1038

998 **Zaffagnini M, De Mia M, Morisse S, Di Giacinto N, Marchand CH, Maes A, Lemaire SD, Trost P** (2016)
999 Protein S-nitrosylation in photosynthetic organisms: A comprehensive overview with future
1000 perspectives. *Biochim Biophys Acta* **1864**: 952-966

1001 **Zaffagnini M, Morisse S, Bedhomme M, Marchand CH, Festa M, Rouhier N, Lemaire SD, Trost P** (2013)
1002 Mechanisms of nitrosylation and denitrosylation of cytoplasmic glyceraldehyde-3-phosphate
1003 dehydrogenase from Arabidopsis thaliana. *J Biol Chem* **288**: 22777-22789

1004 **Zhang L, Happe T, Melis A** (2002) Biochemical and morphological characterization of sulfur-deprived and
1005 H₂-producing Chlamydomonas reinhardtii (green alga). *Planta* **214**: 552-561

1006 **Zhang P, Allahverdiyeva Y, Eisenhut M, Aro EM** (2009) Flavodiiron proteins in oxygenic photosynthetic
1007 organisms: photoprotection of photosystem II by Flv2 and Flv4 in Synechocystis sp. PCC 6803.
1008 *PLoS ONE* **4**: e5331

1009 **Zhang Z, Shrager J, Jain M, Chang CW, Vallon O, Grossman AR** (2004) Insights into the survival of
1010 Chlamydomonas reinhardtii during sulfur starvation based on microarray analysis of gene
1011 expression. *Eukaryot Cell* **3**: 1331-1348

1012 **Zhao DY, Tian QY, Li LH, Zhang WH** (2007) Nitric oxide is involved in nitrate-induced inhibition of root
1013 elongation in Zea mays. *Ann Bot* **100**: 497-503

1014 **Zhao T, Wang W, Bai X, Qi Y** (2009) Gene silencing by artificial microRNAs in Chlamydomonas. *Plant J* **58**:
1015 157-164

1016

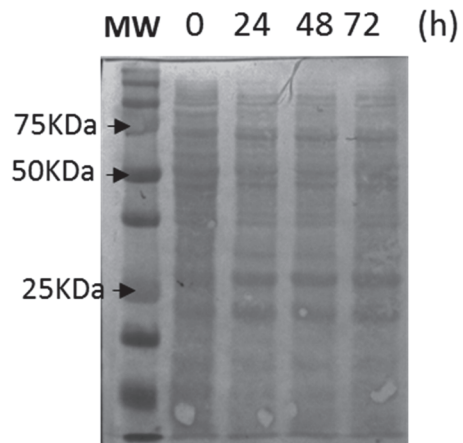


Figure S1. Total protein profiles during sulfur starvation.

Protein degradation was assessed on global extracts of cells kept in TAP-S and low light during 72 hours, harvested at indicated time points and stained with Ponceau red onto nitrocellulose membrane.

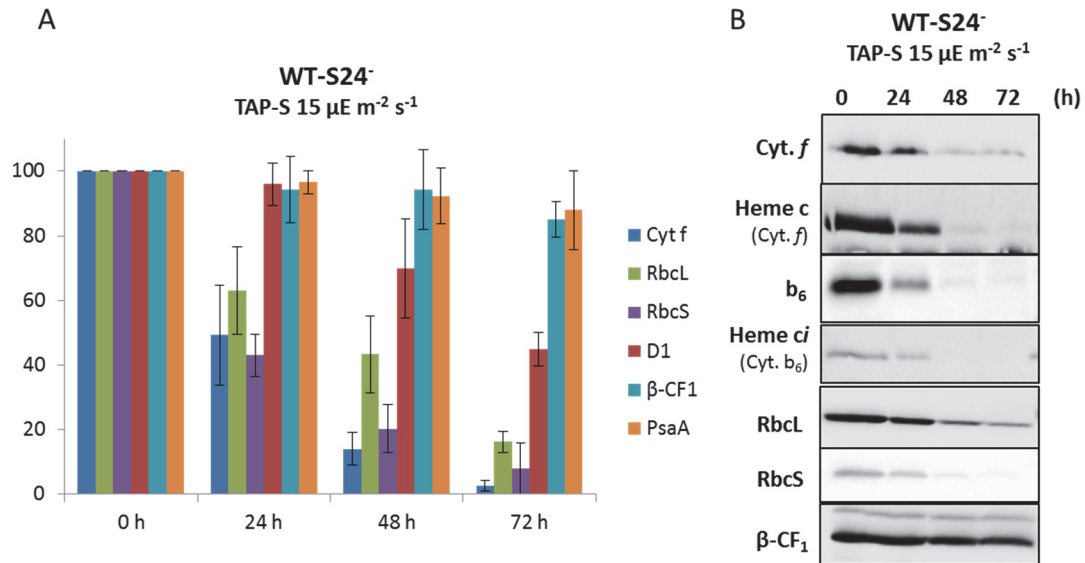


Figure S2. Photosynthetic complex accumulation upon sulfur starvation and correlation between cytochrome *b₆f* degradation and inactivation.

(A) Relative band intensity of indicated antibodies for WT-S24⁻ cells starved in TAP-S medium at 15 $\mu\text{E m}^{-2} \text{s}^{-1}$. Data show the mean of three independent experiments \pm SEM, values are normalized to 100% for T₀.

(B) Whole protein extracts from WT-S24⁻ cells starved in TAP-S at 15 $\mu\text{E m}^{-2} \text{s}^{-1}$, harvested at indicated time points and probed with indicated antibodies and by heme peroxidase activity detection using enhanced chemiluminescence (ECL). β -CF₁ is an internal loading control. Samples were loaded at least three times on mirror gels.

TAP-S

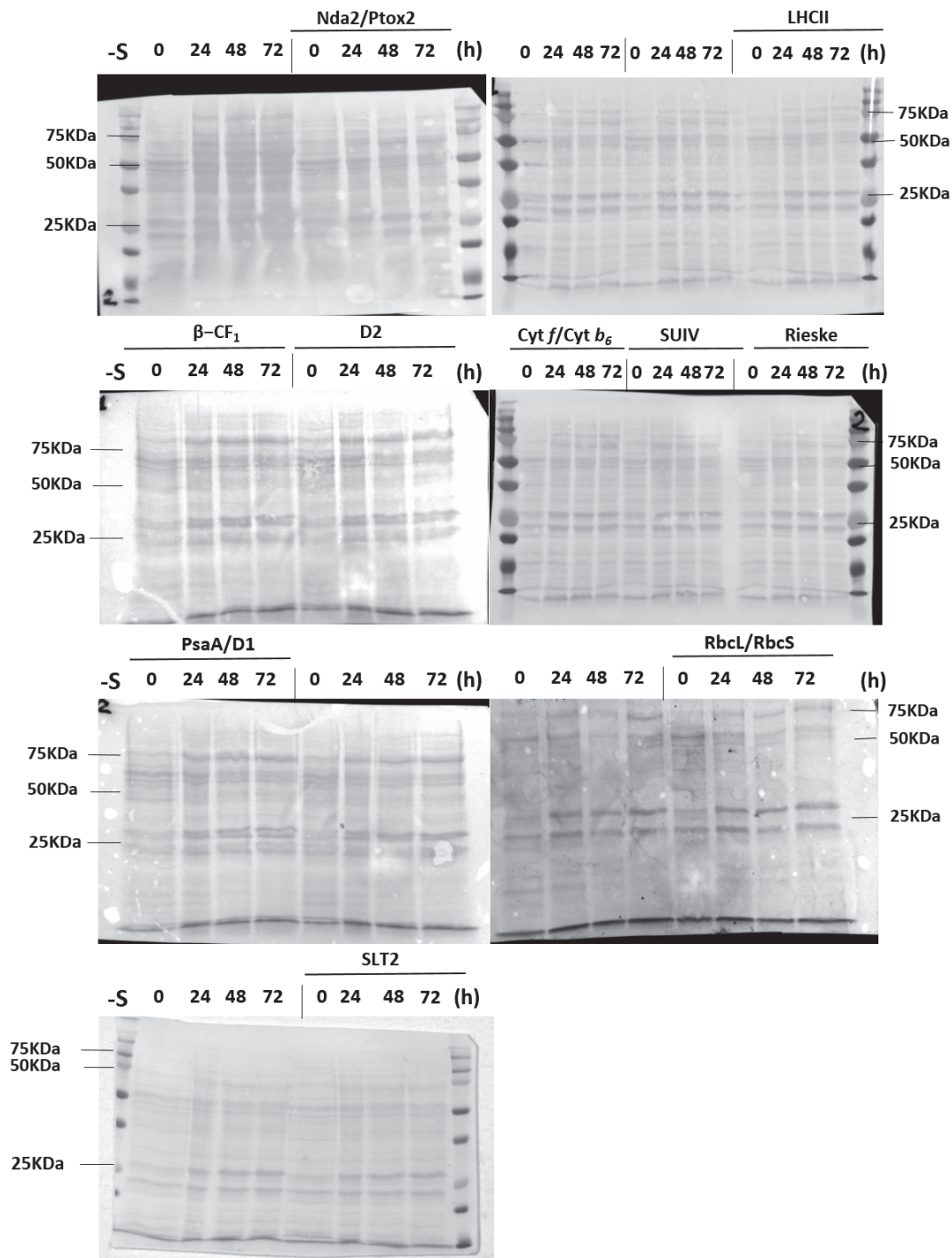


Figure S3A. Protein loading control with Ponceau red staining for TAP-S.

One set of nitrocellulose membranes used to assemble figure 1 (TAP-S medium) and stained with Ponceau red to verify correct gel loading. Gels were loaded on a chlorophyll content basis. For chlorophyll concentration determination, optical density at 680 nm was determined. 3-5 μ g of chlorophyll are typically loaded per lane. The proteins probed in figure 1 are indicated for each membrane.

M.M.-S

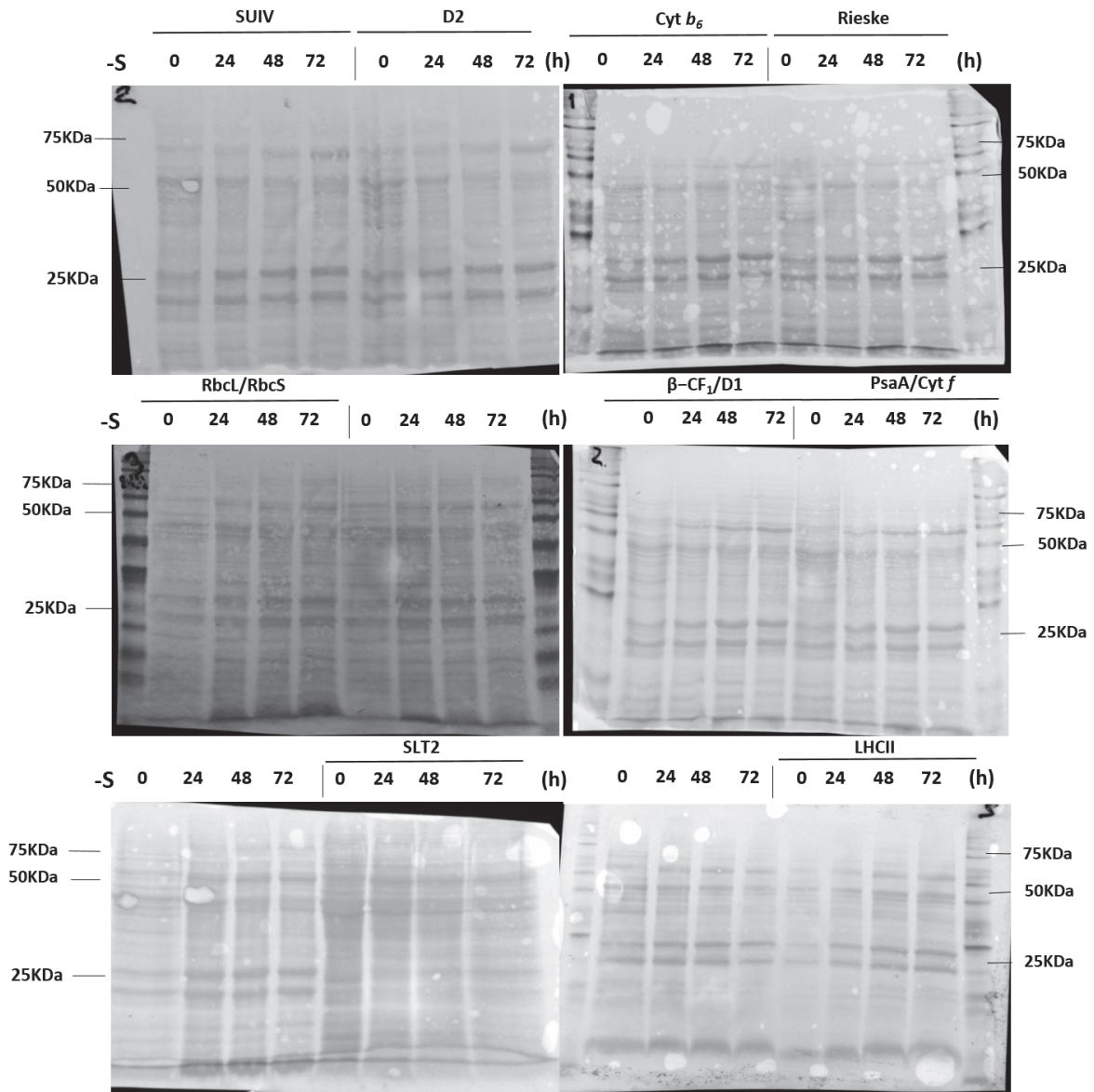


Figure S3B. Protein loading control with Ponceau red staining for M.M.-S.

One set of nitrocellulose membranes used to assemble figure 1 (minimal medium, M.M.-S) and stained with Ponceau red to verify correct gel loading. Gels were loaded on a chlorophyll content basis. For chlorophyll concentration determination, optical density at 680 nm was determined. 3-5 μg of chlorophyll are typically loaded per lane. The proteins probed in figure 1 are indicated for each membrane.

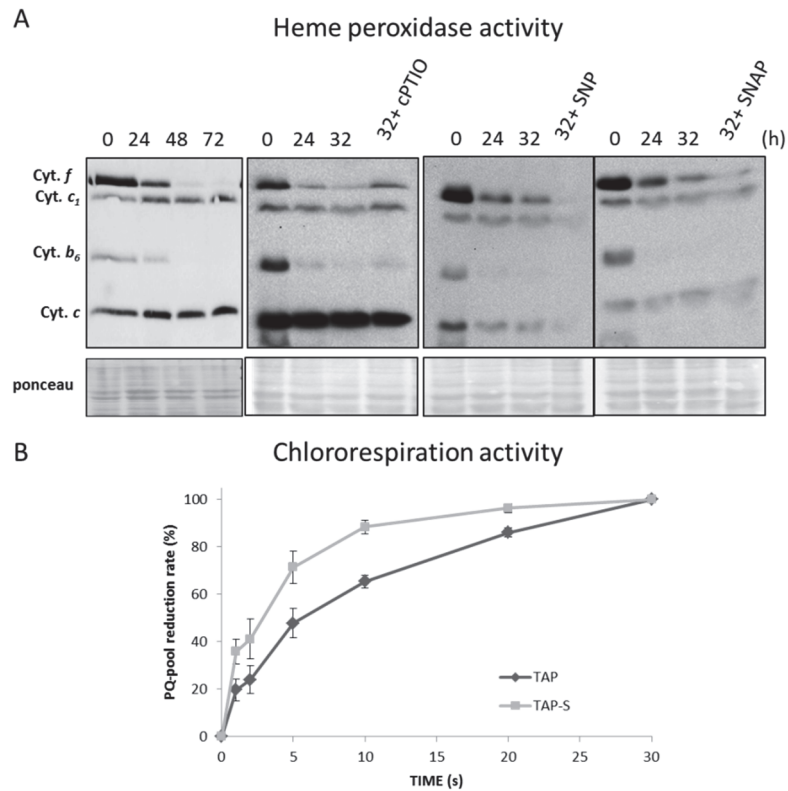


Figure S4: respiratory metabolism and chlororespiration

(A) Peroxidase activity of heme c groups from total extracts of WT-S24 starved in heterotrophy. The peroxidase activity was assessed as in Vargas et al., 1993 at indicated time points in absence or presence of NO donors (either SNP or SNAP) or of the NO scavenger cPTIO.

(B) Chlororespiratory activity of Δ petA cells in TAP and in TAP-S after 48 hours of starvation.

Measurements were taken as in (Houille-Vernes et al., 2011). Results show the mean of 3 independent experiments \pm SEM. Data were normalized to F_M taken in TAP conditions.

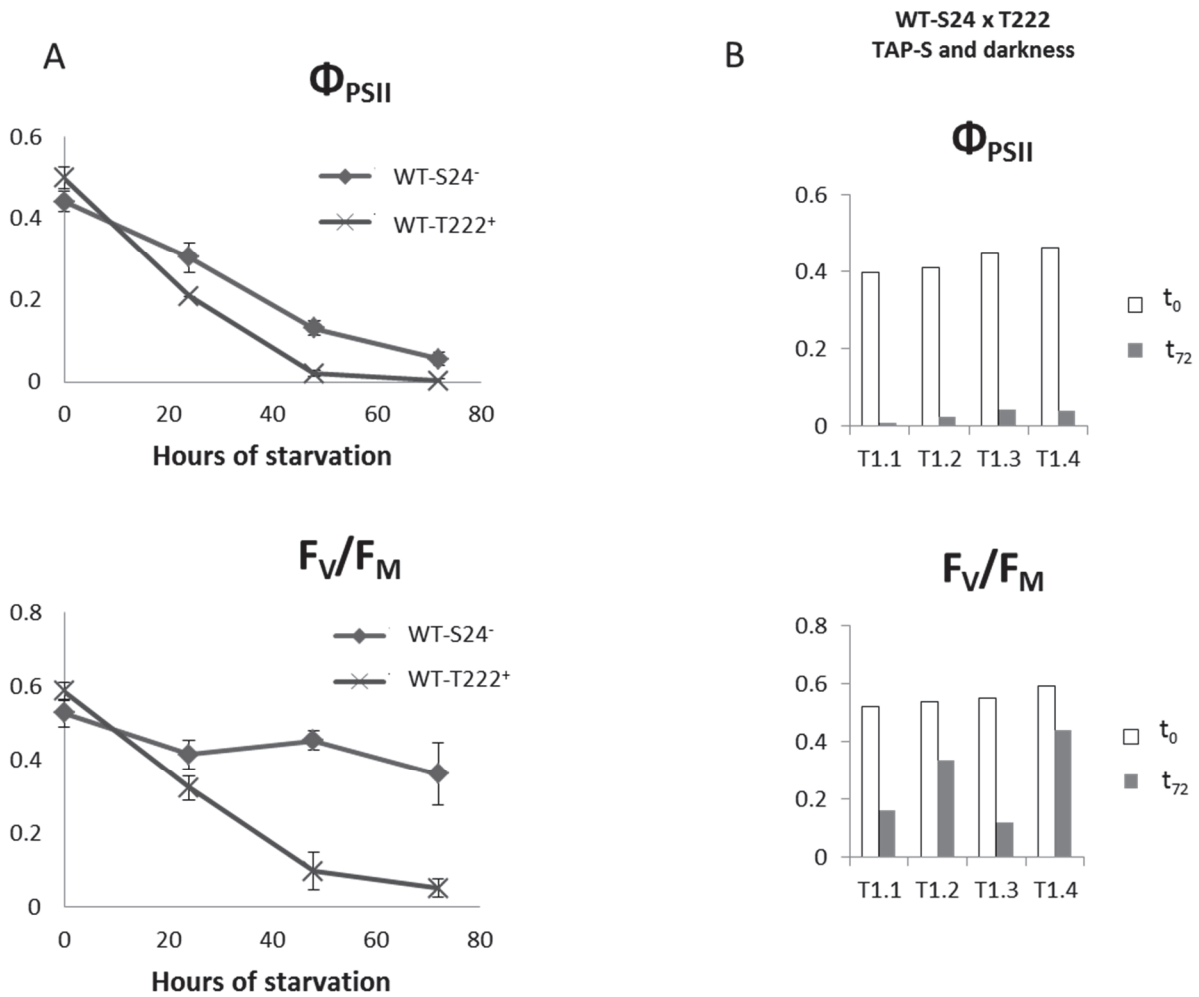


Figure S5. Effects of sulfur deprivation in darkness and in heterotrophy on WT-S24⁻ and WT T222⁺.

(A) Evolution of Φ_{PSII} and F_V/F_M during sulfur starvation of strain WT-S24⁻ (diamonds), and WT T222⁺ (stars) in TAP-S and complete darkness. Data represent the mean of 3 independent experiments \pm SEM.

(B) Evolution of Φ_{PSII} and F_V/F_M of one representative tetrad obtained from crossing of WT-S24⁻ and WT T222⁺.

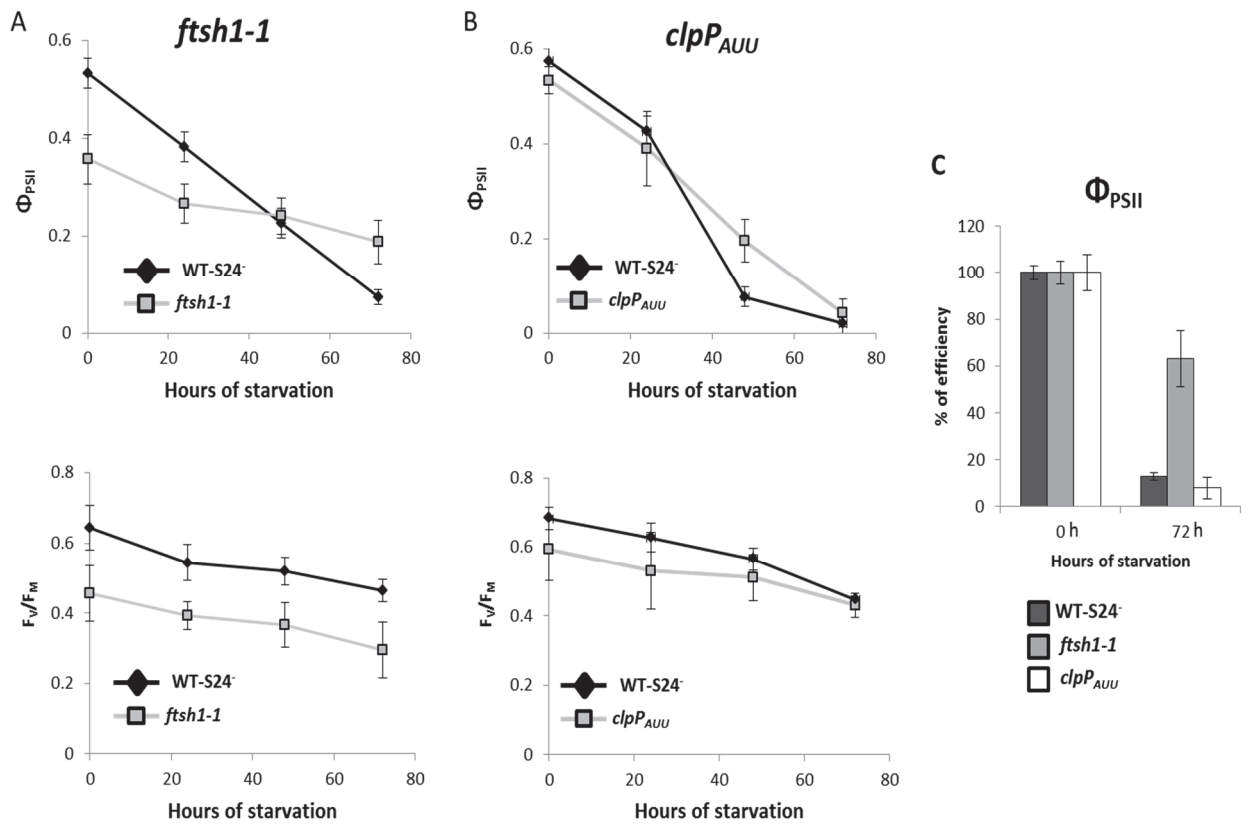


Figure S6. Sulfur starvation on the *ftsh1-1* and *clpPAUU* mutants, defective for protease function.

(A) Comparison of photosynthetic parameters evolution, Φ_{PSII} (top) and F_v/F_m (bottom), for WT-S24⁻ and *ftsh1-1* under starvation in TAP-S and $15 \mu E \cdot m^{-2} \cdot s^{-1}$.

(B) Comparison of photosynthetic parameters evolution, Φ_{PSII} (top) and F_v/F_m (bottom), for WT-S24⁻ and *clpPAUU* under starvation in TAP-S and $15 \mu E \cdot m^{-2} \cdot s^{-1}$.

(C) Residual photosynthetic efficiency (as % of the initial efficiency) after 72h of starvation between WT-S24⁻, *ftsh1-1* and *clpPAUU*.

Data represent the mean of 5 independent experiments \pm SEM.

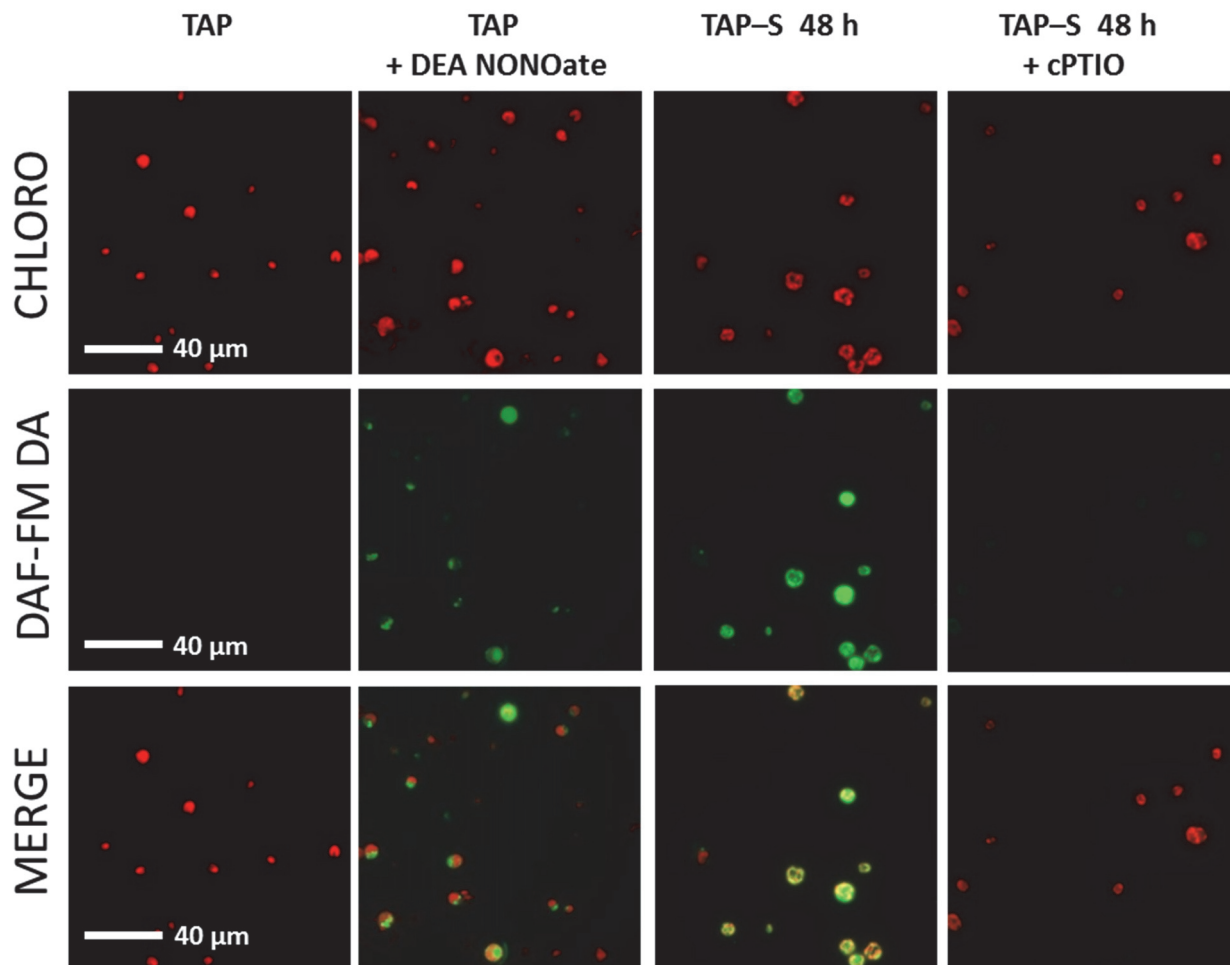


Figure S7. DAF-FM DA fluorescence can be seen only in presence of nitric oxide or under sulfur starvation.

Visualization of NO production *in vivo*, using the DAF-FM DA (5 μ M) probe. Cells were harvested and observed with a fluorescence microscope after washing step and 10-fold concentration. CHLORO, chlorophyll autofluorescence; DAF-FM DA, NO-dependent green fluorescence; MERGE, chlorophyll and NO-dependent signals visualized together.

From left to right panels: Cells in replete medium; cells in replete medium incubated with DEA NONOate (0.1 mM); starved cells after 48 hours; starved cells after 48 hours incubated 1 hour with NO-scavenger cPTIO (0.2 mM).

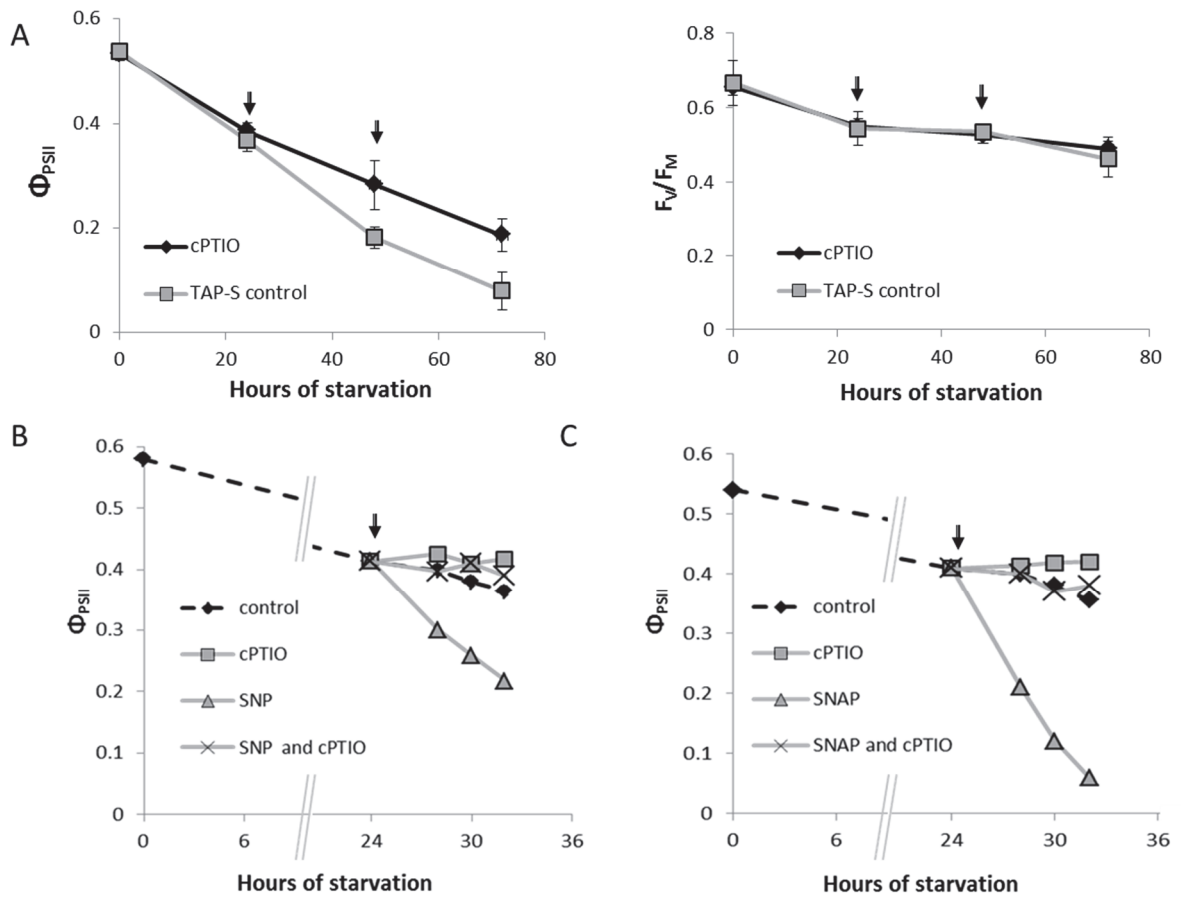


Figure S8. Effects on photosynthetic parameters of cPTIO alone or in the presence of NO donors.

(A) Φ_{PSII} and F_v/F_M evolution measured after addition of cPTIO (0.1 mM) every 24 hours. Data show the mean of three independent experiments \pm SEM.

(B) Effects on photosynthetic efficiency of SNAP (0.05 mM) and cPTIO (0.2 mM), added alone or together.

(C) Effects on photosynthetic efficiency of SNAP (0.5 mM) and cPTIO (0.2 mM), added alone or together.

Black arrows indicate drug addition, experiments were performed in TAP-S at $15 \mu E \cdot m^{-2} \cdot s^{-1}$.

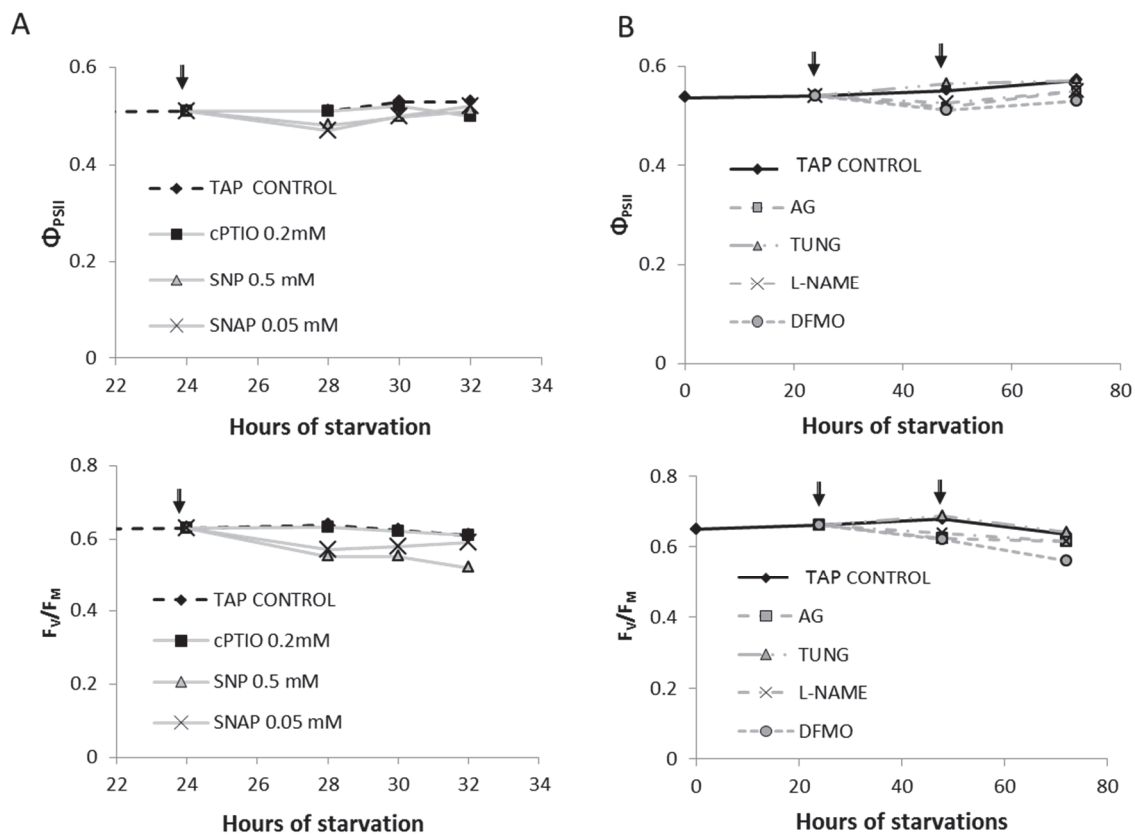


Figure S9. Effects of NO-donors/scavenger and NO-synthesis inhibitors on photosynthetic parameters in sulfur replete conditions.

(A) Effects of NO-scavenger/donors on Φ_{PSII} (top) and F_v/F_m (bottom) of WT-S24⁻ cells kept in TAP at $15 \mu E \cdot m^{-2} \cdot s^{-1}$.

(B) Effects of NO synthesis inhibitors (1 mM final concentration for all) on Φ_{PSII} (top) and F_v/F_m (bottom) of WT-S24⁻ cells kept in TAP at $15 \mu E \cdot m^{-2} \cdot s^{-1}$.

Arrows indicate drugs addition.

TAP-S

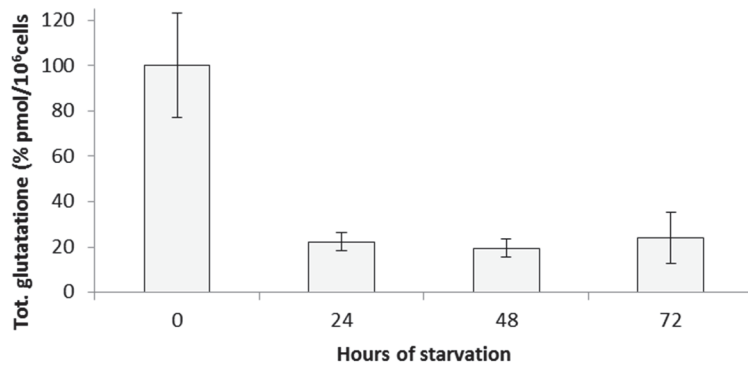


Figure S10: Total glutathione content of cell extracts during sulfur starvation

Samples were harvested at indicated times during sulfur starvation in TAP-S and analyzed as in (Queval and Noctor, 2007) and (Pérez-Martin et al., 2014). Data represent the mean of 3 independent experiments \pm SEM.